ANALYSIS OF HEAT STORAGE WITH A THERMOCLINE TANK FOR CONCENTRATED SOLAR PLANTS

Proposal of a simulation model and design of an alternative storage system for AndaSol I solar plant

Author: Albert Graells Vilella

Tutor: Mr. Serhat Yesilyurt

Sabanci University

Industrial Engineering

Spring semester 2014

TABLE OF CONTENTS

ABSTRACT

The storage system in a concentrated solar plant is considered an important concern to increase the capacity factor of the plant by producing power during the night or in cloudy days. This paper presents different storage materials, and introduces several storage systems available. Moreover, the paper is focused on the analysis of a thermocline system, which consists on a single tank that typically works with molten salt and quartzite rock as storage media. A simulation model of heat charging and discharging process is designed with the numerical solution of non dimensional Schumann equations. These equations describe the heat transfer between the thermal fluid and the filler material. The model has been validated with experimental data, and the results have been compared with other models. Then, the proposed model is then used to design an alternative storage system for the solar plant AndaSol I. Moreover, the model has been used analyze the influence of the ratio between height and diameter of the tank in the energy storage efficiency. Finally, a comparison between three thermal storage fluids has been made in order to find out which Heat Transfer Fluid is better for the designed thermal storage tank.

NOMENCLATURE

a_f	Cross sectional area of storage tank (m^2)
C_p	Specific heat (J/kg·K)
D	Diameter of the storage tank (m)
d	Nominal diameter (m)
E	Energy (J)
f_s	Surface shape factor (2-3)
H	Height of the storage tank (m)
H_{CR}	Dimensionless parameter
h	Enthalpy (J/kg)
h_i	Interstitial heat transfer coefficient ($W/m^3 \cdot K$)
k	Thermal conductivity (W/m·K)
M	Mass (kg)
$\dot{m}$	Mass flow rate (kg/s)
N	Number of nodes
Nu_i	Nusselt number
P	Power (W)
Pr	Prandtl number
p	Pressure (Pa)
Q	Thermal energy (J)
R	Radius of the storage tank (m)
Re	Reynolds number
r	Equivalent radius of a rock (m)
r_{char}	Characteristic radius by Nellis and Klein, Hydraulic radius (m)
S	Surface area (m^2)
T	Temperature (K)
t	Time (s)
U	Overall heat transfer coefficient ($W/m^2 \cdot K$)
u	Fluid velocity in the axial direction in the storage tank (m/s)
V	Volume (m^3)
W	Gross turbine output (W)
z	Location along the axis of the tank

Greek symbols

α	Thermal diffusion (m^2/s)
ε	Porosity of packed bed in storage tank
η	Efficiency
Ω	Turbine blade speed (rpm)
□	Dynamic viscosity (Pa·s)
τ_r	Dimensionless parameter
$\boldsymbol{\rho}$	Density (kg/m^3)
Θ	Dimensionless temperature

Subscript

0	Rated condition
c	Cold
e	Electric
eff	Effective
f	Thermal fluid
HX	Power block heat exchangers
h	Hot
heel	Liquid heel
in	Inlet
init	Initial
j	Discretized variable of time
k	Discretized variable of space, Node position
l	Molten Salt
r	Rocks
rec	Receiver
s	Filler material
T	Thermal
t	Turbine
z	Location along the axis of the tank

Superscript

*	Dimensionless values

PART 1

1. Introduction

It is widely known that we live in an unsustainable world, and that the increase of population predicted for the next decades will require much more amount of energy. Moreover, the natural resources are limited and some of them are beginning to disappear. For these reasons, the goals for the next years in the Energetic field are clear and agreed for the most part of institutions and governments: A great improve on the efficiency of energy processes and an increase in the use of renewable energies which not require limited natural resources.

Therefore, solar power plants are a good alternative for conventional thermal power stations to produce sustainable electricity. However, they should deal with the problem of producing power during cloudy periods. Consequently, to improve the efficiency of solar plants, most of investigations focus efforts on the thermal storage system. For this reason, there are already quite a few different types of storage systems which will be presented on the next pages. Nevertheless, the thermocline tank system seems to highlight from the other systems because of his low-cost in comparison with the two tanks system.

In the following pages, one can come across different systems of heat storage with different materials. Besides this, two approximations to a thermocline tank are presented through a pair of models from different papers. Moreover, with the previous influences, a new simulation of charge and discharge process in a thermocline tank will be presented, and used in the design of an alternative heat storage system in AndaSol I solar plant. The storage system currently used in this plant consists on two separate tanks which store the hot and cold fluid independently. Therefore, a storage system with one single thermocline tank with the same heat capacity will be proposed as a low-cost alternative.

2. State of the art on high temperature thermal energy storage for power generation [1]

2.1 Thermal energy storage

2.1.1 Definition

Thermal energy storage (TES) allows large-scale switching. Consequently, these systems increase significantly the effectiveness of the power plants. In other words, it is a method to take more profit from the solar energy and by this way; the plants can produce electricity during the night or in cloudy days. Therefore, storage systems are a useful way to increase the capacity factor of a solar plant.

There are three different types of TES systems: sensible heat storage, latent heat storage and chemical heat storage. Nevertheless, sensible storage systems are the ones mainly used. The concept that defines this systems is the sensible heat which is the energy absorbed by a material as its temperature is increased. Besides this, the energy required to convert the phase of a material is called heat of fusion (solid to liquid) or heat of vaporization (liquid to gas). Latent heat storage systems use this concept to storage thermal energy. Finally, the last type of systems is related to reversible endothermic chemical reactions. A reversible reaction allows recuperating the heat (synthesis reaction) that previously has been used to dissociate a chemical product.

The complete storage process is divided in three steps: charging, storing and discharging. However, as will be seen later, some of these steps can be simultaneous. For example, it is frequently common to charge the storage media while producing steam and so, electricity.

2.1.2 Design criteria

The most important feature in the design of a TES is the thermal capacity. Besides this, there is also important to consider several other considerations like the cost-benefit, the technical criteria and the environmental criteria.

The cost of a TES system depends directly on the storage material, the heat exchanger between the heat transfer fluid (HTF) and the storage media and the cost of the space. It is appropriate to optimize the cost of each of these items.

The concepts to bear in mind when designing the technical characteristics of the TES are the followings:

- Storage capacity: high energy density in the storage material.
- Efficiency: good heat transfer between the HTF and the storage media.
- Stability: mechanical and chemical stability of the storage media.
- Safety: compatibility between the HTF, the heat exchanger and the storage media.
- Low thermal losses.
- Ease of control.

Finally, the concepts related with the technology are:

- Operation strategy.
- Maximum load.
- Nominal temperature.
- Specific enthalpy drops in load.

2.1.3 Storage media

2.1.3.1 Sensible heat storage: There are two types of storage media. On the one hand, there is the solid media which consists mainly on concrete and castable ceramics. In this case, it is usually used in packed beds which require a fluid to exchange heat. If the fluid is a liquid, the heat capacity of the solid media cannot be neglected and it is called dual storage system.

On the other hand, the storage can be made with liquid media. Frequently, the materials are molten salts, minerals oils or synthetic oils. From this type of storage media, it is important to highlight the natural stratification because of the difference density between the hot and cold fluid.

2.1.3.2 Latent heat storage: The materials used in this case are called phase change materials (PCM) and it is mainly used the solid-liquid transition. This change of phase involves a thermal heat called heat of fusion. Besides this, there is also the change of phase from liquid to vapour which is defined by the heat of vaporization.

This method is not very developed and that is the reason why their use is not very common. Nevertheless, it is important to highlight that it allows storing a lot of thermal energy in smaller volumes than the sensible heat storage systems. Consequently, the cost of the storage media can be reduced. Besides this, it is also important to consider the complexity on the design of the heat transfer and the storage media.

2.1.3.3 Chemical heat storage: This type of storage can be divided in two different reactions. Firstly, there is a need of heat to excite and endothermic reaction. This heat will be provided by the sun. Then, if the reaction is reversible, the heat can be recovered by the reverse reaction.

This system is called reversible thermochemical reaction (RTR) and one of the advantages is the high storage energy density. However, as in the latent heat storage media, the system is not yet developed and therefore, its use is insignificant.

2.1.4 Storage concept

2.1.4.1 Active storage direct system: The active storage systems are characterized by forced heat exchange into the storage media which circulates by itself through a heat exchanger. A direct system means that the HTF is the same as the storage material and it is usually store in two different tanks which store the hot and cold media separately.

2.1.4.2 Active storage indirect system: In this case, the HTF is different from the storage medium. Moreover, the storage can be done in two tanks or in a single tank. The advantage of the single solar tank is the reduced cost, but the two tanks solar systems allow to store separately the hot and cold storage material which is a safety method. Finally, it is important to know that the single tank is commonly called thermocline. In this system, the hot fluid is stored on the top of the tank and the cold on the bottom because of the density difference. The stratification along the length of the tank is due to a filler materials store inside the tank. Usually, quartzite rock and silica sand are used as filler materials. Furthermore, it is necessary to consider the filler material as the primary thermal storage medium.

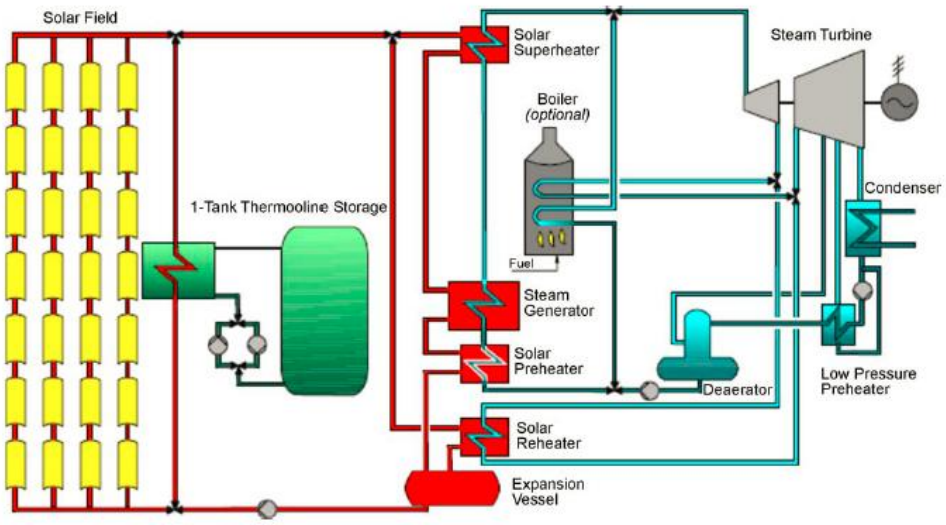

Fig. 1. Scheme of the installation of a thermal power plant with thermocline storage system [2].

2.1.4.3 Passive storage system: In the passive storage systems, the storage media does not circulate. The HTF circulates through the storage media only for charging and discharging the tank. This system is usually called regenerators and it works as a dual medium storage system.

Besides this, the solid storage systems are the most used for passive storage and usually, concrete or castable ceramics are used as the storage media. Also, it is possible to use PCM as storing materials, but the technology required for using this concept is not yet developed.

2.2 Materials

2.2.1 Sensible heat storage materials

This group of materials store thermal energy because of the increase of temperatures without any change of phase. The amount of energy stored can be expressed as:

$$Q = M \cdot C_P \cdot \Delta T$$

Q ≡ thermal energy stored [J]

M ≡ mass of the storage material [kg]

C_P ≡ specific heat [J/kg·K]

ΔT ≡ increase of temperature [K]

If the mass is expressed with the density and the volume, the expression becomes the following:

$$Q = \rho \cdot C_P \cdot V \cdot \Delta T$$

$\boldsymbol{\rho}$ ≡ density of the storage material [kg/m^3]

V ≡ volume occupied by the storage material [m^3]

This equation permits to recognize a concept very important to bear in mind when choosing the storage material. It is called thermal capacity and it is expressed as the product between the density and the specific heat ($\boldsymbol{\rho}\cdot C_P$).

Regarding about the solid materials, the most used are concrete and castable ceramics. As we can see in the following tables, this materials stand out for their low price and good thermal conductivities.

Besides this, the liquid materials more used are the molten salts. Nevertheless, it is convenient to pay attention at two aspects when using molten salts. They used to cause corrosion problems and their freezing point can be critic sometimes because it is high. The principal molten salts are the solar salt (60% $NaNO_3$, 40%KNO_3) and the salt called HitecXL (48% $Ca(NO_3)_2$, 7% $NaNO_3$, 45% KNO_3).

Material	Castable ceramic	High temperature concrete
Density [kg/m^3]	3500	2750
Specific heat at 350 °C [J/kg K]	866	916
Thermal conductivity at 350 °C [W/m K]	1.35	1.0
Coefficient of thermal expansion at 350 °C [10^{-6}/K]	11.8	9.3

Table 1. Properties of sensible heat solid storage materials [1]

Storage medium	Temperature		Average density (kg/m^3)	Average thermal conductivity (W/m K)	Average heat capacity (kJ/kg K)	Volume specific heat capacity (kWh$_t$/m^3)	Media costs per kg (US$/kWh$_t$)	Media costs per kWh$_t$ (US$/kWh$_t$)
	Cold (°C)	Hot (°C)						
HITEC solar salt	120	133	–	–	–	–	–	–
Mineral oil	200	300	770	0.12	2.6	55	0.30	4.2
Synthetic oil	250	350	900	0.11	2.3	57	3.00	43.0
Silicone oil	300	400	900	0.10	2.1	52	5.00	80.0
Nitrite salts	250	450	1825	0.57	1.5	152	1.00	12.0
Nitrate salts	265	565	1870	0.52	1.6	250	0.50	3.7
Carbonate salts	450	850	2100	2.0	1.8	430	2.40	11.0
Liquid sodium	270	530	850	71.0	1.3	80	2.00	21.0

Table 2. Properties of sensible heat liquid storage materials [1]

2.2.2 Latent heat storage materials

The solid-liquid transition is the most interesting phase change to use because it is more efficient than the sensible thermal storage systems. One of the principal advantages is the lower interval of operation temperatures between charging and discharging. Moreover, the energy density is also higher compared to sensible systems.

Nevertheless, there is also one problem that must be worked out: the low thermal conductivity. In other words, this problem explains the slow charging and discharging rates. For arranging this inconvenient, there are two different solutions: the improvement of the heat transfer using mass transfer and the increase of thermal conductivity by adding objects with larger thermal conductivity. Consequently, one of the most common materials used is the PCM/graphite which is a composite of PCM with portions of graphite.

2.2.3 Chemical heat storage materials

These materials are not yet enough developed, but it is important to consider them because of his potentially high energy density. However, there are several reactions that have been investigated: reactions metal oxide/metal (SnO_x/Sn) and ammonia (NH_3).

$SnO_2 + 2CH_4 + q \rightarrow Sn + 2CO + 4H_2$

$Sn + 2H_2O \rightarrow SnO_2 + 2H_2 + q$

$2NH_3 + q \rightarrow N_2 + 3H_2$

$N_2 + 3H_2 \rightarrow 2NH_3 + q$

2.2.4 Material properties

To study the applications of PCM, it is convenient to look at the thermal properties such as the energy storage capacity and the thermal conductivity. The energy storage capacity is expressed by the enthalpy variation between two temperatures, including the sensible and the latent energy. That is the reason why it is needed the enthalpy vs. temperature curve because it is important to know the evolution of thermal properties with the temperature during the charging and discharging process.

Besides this, during the designing of the heat exchanger, the thermal conductivity is commonly used to evaluate the rate of the heat exchanger. The following equation is used to evaluate the thermal conductivity:

$$k = \rho \cdot C_P \cdot \alpha$$

k ≡ thermal conductivity [W/m·K]

$\boldsymbol{\rho}$ ≡ density of the storage material [kg/m^3]

C_P ≡ specific heat [J/kg·K]

α ≡ thermal diffusion [m^2/s]

As we can see, the thermal conductivity is directly proportional to the thermal diffusion so that measuring experimentally the thermal diffusion; the thermal conductivity can be evaluated.

3. Modelling of high temperature storage systems

The following two models were implemented to simulate and analyse the heat storage and delivery of a thermocline with solid filler material. In both of them, the solid filler material is quartzite rock and the HTF is a commercial nitrate salt mixture composed by 60 wt% $NaNO_3$ and 40 wt% KNO_3.

Moreover, the two methods use the Schumann equations which describe the heat transfer between the fluid and a packed bed. However, the second analysis does not consider the effective thermal conductivity of the rock because it can be lumped. Besides this, the principal difference between both methods is that the second one works with dimensionless variables which simplify considerably the governing equations.

3.1 Reduced-order finite-volume model [3]

3.1.1 Thermocline tank model

The salt remains liquid above 220ºC. Thus, the operation temperature span is 300-600ºC in order to never reach the freezing point. The physical properties of the molten salt are a function of the temperature. Below we can see the expression of these properties:

$$\rho_l = 2090 - 0{,}636 \cdot T_l \quad (1.1)$$

$$k_l = 0{,}443 + 1{,}9 \cdot 10^{-4} \cdot T_l \quad (1.2)$$

$$\mu_l = 0{,}022714 - 1{,}20 \cdot 10^{-4} \cdot T_l + 2{,}281 \cdot 10^{-7} \cdot T_l^2 - 1{,}474 \cdot 10^{-10} \cdot T_l^3 \quad (1.3)$$

$\rho_l \equiv$ density of the molten salt [kg/m^3]

$k_l \equiv$ thermal conductivity of the molten salt [W/m·K]

$\mu_l \equiv$ viscosity of the molten salt **[Pa·s]**

$T_l \equiv$ temperature of the molten salt [ºC]

$C_{pl} \equiv$ specific heat of the molten salt. **1520 J/kg·K**

Besides this, the properties of the solid filler material are assumed constants in the entire operation span.

$\boldsymbol{\rho}_s \equiv$ density of the quartzite rock bed. **2500 kg/m^3**

$k_s \equiv$ thermal conductivity of the quartzite rock bed. **5 W/m·K**

$C_{ps} \equiv$ specific heat of the quartzite rock bed. **830 J/kg·K**

$T_s \equiv$ temperature of the quartzite rock bed [ºC]

$\varepsilon \equiv$ porosity of the quartzite rock bed. **0,22**

Because of the density variation of the molten salt, the tank cannot be considered as a control volume. The density of the molten salt is lower when the tank is hot. For this reason, at that moment the liquid level inside the tank rises, while if the tank is cold, the liquid level falls.

Consequently, to prevent the dryout of the porous region, there is an additional volume of the molten salt which is maintained above. The temperature of this region is very important because it represents de temperature available for steam generation.

3.1.1.1 Porous region: the following equations define the heat energy transport between the HTF and the filler material in the porous region.

$$\frac{\partial[\varepsilon\rho_l C_{pl}(T_l - T_c)]}{\partial t} + \nabla\cdot\left[\rho_l u C_{pl}(T_l - T_c)\right] = \nabla\cdot\left(k_{eff}\nabla T_l\right) + h_i(T_s - T_l) \quad (1.4)$$

$$\frac{\partial[(1-\varepsilon)\rho_s C_{ps}(T_s - T_c)]}{\partial t} = -h_i(T_s - T_l) \quad (1.5)$$

There are several assumptions considered in this model. Firstly, the temperature in each rock is assumed to be homogeneous, the thermal diffusion between the rocks is also negligible, but the thermal diffusion in the liquid region is considered and expressed with the term k_{eff} (effective thermal conductivity).

To solve these equations, the model is reduced to a one-dimensional formulation along the z-axis so that temperature variation in the radial region is considered negligible. Moreover, it is assumed that the tank is well insulated and the flow through the filler bed is laminar. Therefore, the equations (1.4) and (1.5) reduce to the following differential equations:

$$\frac{\partial(\varepsilon\rho_l C_{pl}\theta_l)}{\partial t} + \frac{\partial(\rho_l u C_{pl}\theta_l)}{\partial z} = \frac{\partial}{\partial z}\left(k_{eff}\frac{\partial\theta_l}{\partial z}\right) + h_i(\theta_s - \theta_l) \quad (1.6)$$

$$\frac{\partial[(1-\varepsilon)\rho_s C_{ps}\theta_s)}{\partial t} = -h_i(\theta_s - \theta_l) \quad (1.7)$$

$$\theta = \frac{T-T_c}{T_h-T_c} \quad (1.8)$$

The unknowns of the system will be the temperatures of the molten salt and the solid filler material. By this way, the system can be solved because it is composed by two equations and two unknowns. Before that, it is important to consider how will be evaluated the terms k_{eff}, h_i and u.

$$k_{eff} = k_i \frac{1+2\beta\phi+(2\beta^3-0{,}1\beta)\phi^2+\phi^3 0{,}05\exp(4{,}5\beta)}{1-\beta\phi} \quad (1.9)$$

$$\phi = 1 - \varepsilon \quad (1.10)$$

$$\beta = \frac{k_s-k_l}{k_s+2k_l} \quad (1.11)$$

$$h_i = \frac{Nu_i \cdot k_l}{D_{eff}} \quad (1.12)$$

D_{eff} ≡ effective diameter of the granulated rock

$$Nu_i = 6(1-\varepsilon)[2 + 1{,}1Re^{0,6}Pr^{\frac{1}{3}}] \quad (1.13)$$

$$u_z = \frac{\varepsilon\rho_{l,z}C_{pl}+(1-\varepsilon)\rho_s C_{ps}}{\varepsilon\rho_{l,in}C_{pl}+(1-\varepsilon)\rho_s C_{ps}} \cdot \frac{\rho_{l,in}}{\rho_{l,z}} \cdot u_{in} \quad (1.14)$$

3.1.1.2 Liquid heel: as commented before, it is important to prevent the dryout of the porous bed during the storage. If not, the available energy storage capacity could be reduced and it could be difficult to extract the hot salt from the tank. For this reason, there is a liquid heel at the top of the tank. The height of the heel is not fixed, but the mass and the energy of the heel are known from the porous region model at each time step. Consequently, the temperature of the liquid heel can be evaluated with the expression below. It is important to take care about the meaning of this temperature because it represents the temperatures available for steam generation in the CSP.

$$T_{heel} = T_c + \frac{E_{heel}}{M_{heel}\, C_{pl}} \tag{1.15}$$

3.1.1.3 Model validation: In this project the accuracy of the model was validated comparing the results simulated for a 2.3 MWh_t molten salt tank against experimental data measurements. In the figure 2 is plotted the predicted results with the model and the experimental results. As we can see, the accuracy of the model was notable.

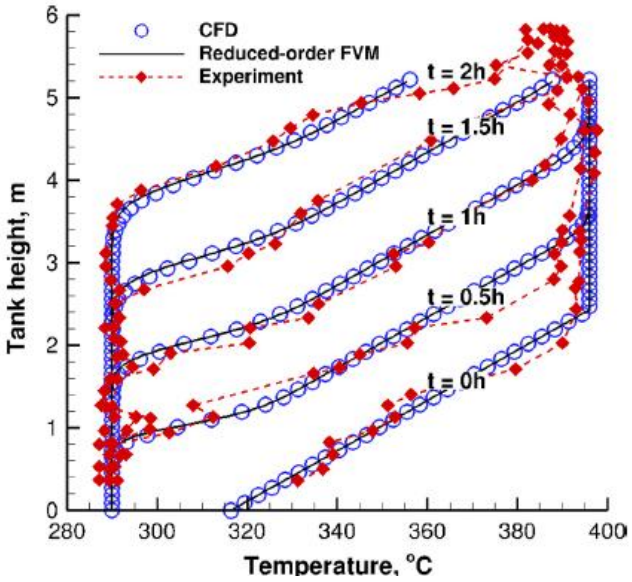

Fig. 2. Stratification temperature of a 2.3 MWh_t thermocline tank during a discharge process. Two numerical simulations and experimental temperature data are performed. [3]

3.1.2 System-level model development

A CSP power plant requires three separate components: the solar collection, the energy storage and the power production. All these components are designed to operate in a 100 MW_e power plant and the study does not consider the possibility of a bypass. In other words, all the heat transfer from solar collection to the power production passes instants before through the thermocline tank.

3.1.2.1 Steam Rankine Cycle: CSP plants produce electricity with a typical Rankine cycle. The hot molten salt generates the steam necessary to move a turbine used for power generation. For producing the steam required the molten salt circulates through three heat exchangers: the pre-heater, the evaporator and the super-heater. The figures (3 and 4) below show the scheme of the power block and the working points in a T-s diagram.

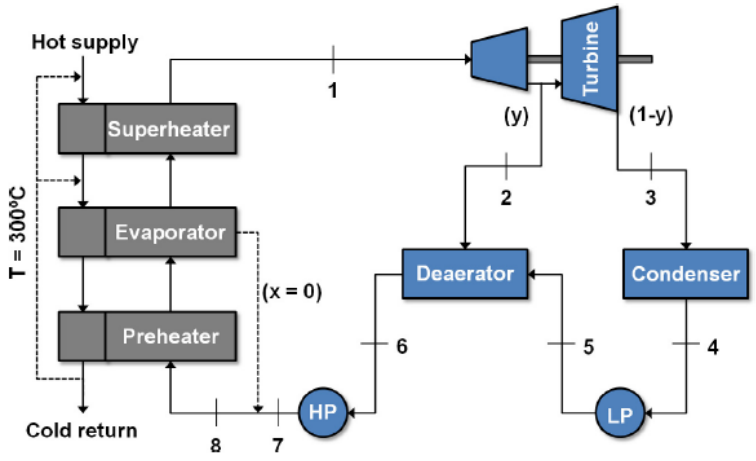

Fig. 3. Design of the steam generation and the power block (Rankine cycle). [3]

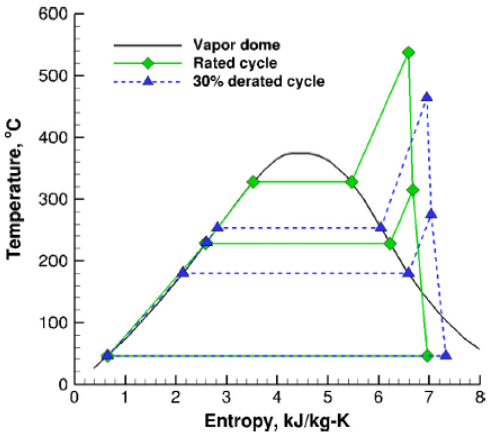

Fig. 4. Temperature-entropy diagram of the steam Rankine cycle. [3]

In the current study, the power block is composed with a non-reheat turbine and a single open feedwater heater. The plant can also work in a state of derated operation for situations in which the temperature of the delivered salt can not reach the 600ºC. There is a reduction of exergy which derives in a reduction on the steam generation and consequently, the inlet temperature of the turbines is reduced. To adapt this reduced temperature of the turbine, the cycle mass flow rate and the pressure are both adjusted. The relationship between the variable mass flow rate and the pressure is the next:

$$\frac{\dot{m}^2}{\dot{m}_0^2} = \frac{p_1^2 - p_2^2}{p_{1,0}^2 - p_{2,0}^2} \tag{1.16}$$

$p_{1,0}$ and $p_{2,0}$ ≡ turbine pressures at normal conditions.

There is also characterized the efficiency of the turbine related with the turbine speed and the entalphy change. Besides this, it is also known the relationship between the efficiency of the pumps and the mass flow rate:

$$\eta_t = \eta_{t,0} - 2\left(\frac{\Omega}{\Omega_0}\sqrt{\frac{\Delta h_{t,0}}{\Delta h_t}} - 1\right)^2 \tag{1.17}$$

$$\frac{\eta_p}{\eta_{p,0}} = 2\frac{\dot{m}}{\dot{m}_0} - \left(\frac{\dot{m}}{\dot{m}_0}\right)^2 \tag{1.18}$$

3.1.2.2 Steam generators: as commented before, the steam generation is produced with three heat exchangers (pre-heater, evaporator and super-heater). Specifically, the span of temperatures for the water to generate the steam is 230-328ºC for the pre-heater, 328ºC to generate the steam in the evaporator at constant temperature and 328-538ºC for the super-heater. Besides this, the molten salt enters the super-heater at 600ºC and exits the pre-heater at 300ºC. In the next table there is the characteristic design of each heat exchanger. The surface areas for the pre-heater and the super-heater were designed with the LMTD method. For the evaporator, the method used was the NTU. These methods are specified in [4].

Heat exchanger	Thermal power, MW	U, W/m^2-K	Area, m^2
Preheater	57.34	1940	580.2
Evaporator	128.4	1392	1042
Superheater	85.12	911	849.8

Table 3. Features desing of the heat exchangers for steam generation. [3]

When the power generation is not at 100% these values change and the heat transfer coefficient (U) becomes a function of the molten salt and steam mass flow rates.

$$\frac{U}{U_0} = \left(\frac{\dot{m}_l}{\dot{m}_{l,0}}\right)^{0.8} \left(\frac{\dot{m}_{steam}}{\dot{m}_{steam\ ,0}}\right)^{0.8} \left(\frac{\dot{m}_{l,0}^{0.8} + \dot{m}_{steam\ ,0}^{0.8}}{\dot{m}_l^{0.8} + \dot{m}_{steam}^{0.8}}\right) \tag{1.19}$$

In this case, the surface area of the pre-heater should decrease in order to maintain the exit salt temperature at 300ºC. For this reason, the pre-heater has a system which allows a variable area.

There is also a relationship between the thermocline tank model, the heat exchangers and the Rankine cycle models. In particular, we can express the output power of the turbine (W) and the molten salt mass flow rate required in the power block related with the hot molten salt temperature:

$$\frac{W}{W_0} = -1.706(\theta_{heel})^3 + 4.406(\theta_{heel})^2 - 2.031(\theta_{heel}) + 0.3307 \tag{1.20}$$

$$\frac{\dot{m}_{HX}}{\dot{m}_{HX\ ,0}} = -0.5976(\theta_{heel})^3 + 0.399(\theta_{heel})^2 + 1.431(\theta_{heel}) + 0.2325 \tag{1.21}$$

Before the start-up of the power generation, the power plant should be synchronised. In this period the power block receives the minimum thermal input (30% load) without producing electricity. When the synchronization is completed, the power production starts with a linear ramp-up. The time for these steps is extremely dependent on the initial turbine temperature which depends on the time passed since the last shutdown. To know the state of the turbine, the initial temperature is classified under three states (Table 4).

Hours after shutdown	Turbine temperature	Warming and synchronization, min	Ramp up, min
<12	Hot	15	25
12–72	Warm	60	100
>72	Cold	110	160

Table 4. Start-up times for each state of the turbine. [3]

3.1.2.3 Solar collection: in the current study the concentrating of the direct sunlight is performed with a central power tower receiver. A large field of heliostats follows the position of the sun and reflects the direct normal irradiance (DNI) to the top of the tower. The molten salt enters the receiver at 300ºC and exits it at 600ºC. Therefore, the mass flow of the molten salt depends on the power received by the sun.

$$\dot{m}_{rec} = \frac{P_{rec}}{C_{pl}\left(T_h - T_{rec,in}\right)} \quad (1.22)$$

3.1.2.4 Model integration: the thermocline tank of the present study is designed to store 6h of thermal energy.

During the daylight hours the molten salt passes through the receiver and charges the thermocline tank. When the storage of the tank could sustain at least 2 hours of power generation, the hot molten salt begins to circulate over the power block in order to initiate turbine start-up and after that, the power production. This condition is considered to avoid frequents flow directions changes that could wear the turbine.

As it is commented before, the plant does not include bypass so that all the molten salt from the solar receiver pass through the tank before the power block. Consequently, the operation condition is dependent on the difference between the flow rate in the solar receiver and in the power block. In other words, to know if the tank is charging, discharging or in stand-by, we should compare the equations 1.21 and 1.22. If the mass flow rate in the solar receiver (equation 1.22) is bigger than the mass flow rate in the power block (equation 1.21), the thermocline tank would be charging. The stand-by situation takes place when the tank has not more usable energy.

The cold salt exiting the tank is limited to 400ºC. It cannot exceed this temperature in order to prevent an overcharge of the storage system. This situation should not be very common because it would mean that the tank is not well designed. For this reason, it is used to oversize the tank during the design process in order to collect the most direct irradiance as possible.

3.1.3 Results of the study

The performance of the power tower plant for five days of June is shown in the figure below:

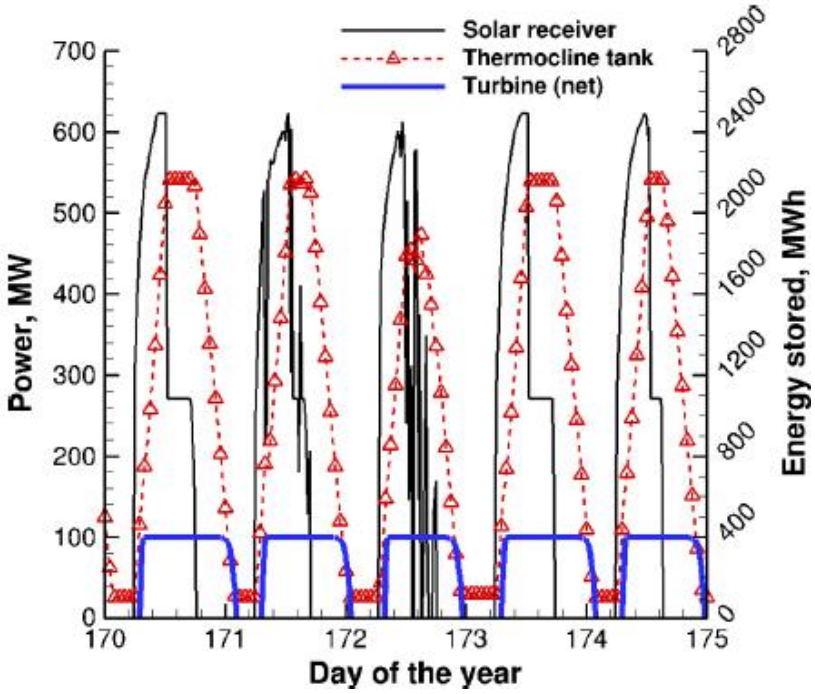

Fig. 5. Power tower plant performance for June 19-23. Net turbine output, solar receiver and energy stored are plotted. [3]

Figure 5 shows that the solar receiver does not work all the day. That is because during the night there is no sun. However, at midday, for some time the tank use to get fully charged and consequently, the solar receiver decreases only to generate enough power for steam production. As it has been commented before, during the design of the plant, these time steps should be minimized as much as possible.

Besides this, figure 5 also shows that the output power production is constant each day. Nevertheless, there are always small periods in which the power plant is not working.

To sum up, the positive effects of the thermocline tank are unquestioned. The installation of the tank allows the plant to produce electricity during the most part of the day and not only during the sunlight hours. In other words, the capacity factor of the plant increases considerably with storage.

$$Capacity\ factor = \frac{1}{W_0}\frac{\int W(t)dt}{\int dt} \tag{1.23}$$

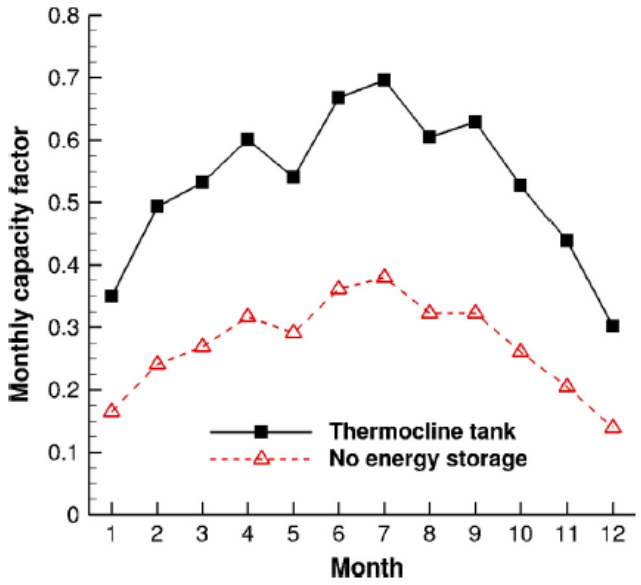

Fig. 6. Power plant capacity factor with and without storage. [3]

In regard to the thermocline tank performance, there is a concept called storage effectiveness that quantifies the ratio of utilizable heat delivered from the tank to the maximum heat available. Utilitzable heat means the molten salt at a acceptable temperature to generate steam. It can also be defined as exergy:

$$\varepsilon_{tank} = \frac{\int \dot{m}_{HX}\, C_{pl}\, (T_{heel} - T_c)\, dt}{\int P_{rec}\, dt + E_{init}} \tag{1.24}$$

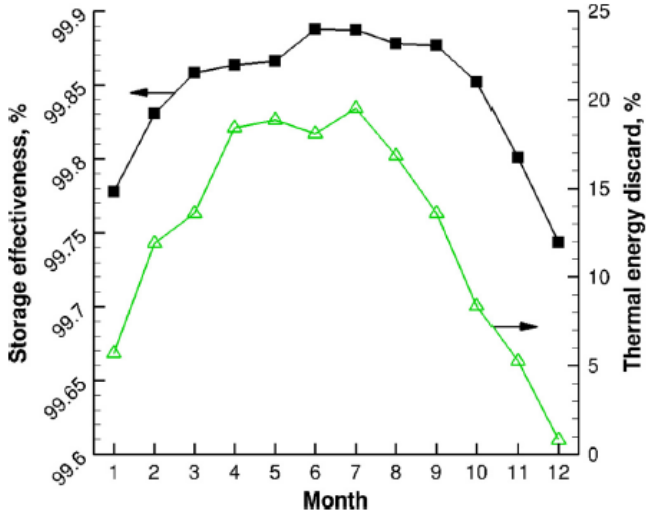

Fig. 7. Thermocline storage performance in a month and thermal enery discard. [3]

The most dependent factors in the impact of a thermocline tank in the power production are the dimensions of the tank and the energy storage capacity. It is important to optimize these terms in order to minimize the time when then the thermocline tank gets full of hot salt. In other words, it is important to have a small thermal energy discard. This concept (Fig. 7) is normalized with respect to the amount of sunlight available for collection. To sum up, this concept helps the designers to know if the storage system is oversized or undersized.

3.2 Non dimensional analysis [5]

Many steps and equations of this analysis are the same as the study before (3.1). Nevertheless, it is useful to view the differences between each method.

3.2.1 Fluid energy balance equation

$$\dot{m}_f \Delta h_{dz} + hS_s\left(T_s - T_f\right)dz = m_f C_f \frac{\partial T_f}{\partial t} \tag{2.1}$$

This equation expresses the energy balance of the fluid in a control volume *dz*. Before exploring the equation, there are some terms that should be defined. It is considered that the section area crossed by the fluid through the axis of the tank is constant and equal to:

$$a_f = \varepsilon \cdot \pi \cdot R^2 \tag{2.2}$$

u ≡ average fluid velocity

The equation 2.1 can be expressed as:

$$\rho_f \varepsilon \pi R^2 u(h_z - h_{z+dz}) + hS_s\left(T_s - T_f\right)dz = \rho_f C_f \varepsilon \pi R^2 \frac{\partial T_f}{\partial t} \tag{2.3}$$

With the definition of the enthalpy, we can express the enthalpy interval with the difference of temperatures between the top and the bottom of the control volume:

$$\frac{hS_s}{\rho_f C_f \varepsilon \pi R^2}\left(T_s - T_f\right) = \frac{\partial T_f}{\partial t} + u\frac{\partial T_f}{\partial z} \tag{2.4}$$

The average fluid velocity in the packed bed is expressed by:

$$u = \frac{\dot{m}}{\rho_f a_f} \tag{2.5}$$

To solve the energy balance equation, it is useful to introduce some dimensionless variables. After that, the governing equation for heat transfer becomes:

$$\theta_f = \frac{T_f - T_c}{T_h - T_c} \tag{2.6}$$

$$\theta_s = \frac{T_s - T_c}{T_h - T_c} \tag{2.7}$$

$$z^* = \frac{z}{H} \tag{2.8}$$

$$t^* = \frac{t}{\left(\frac{H}{u}\right)} \tag{2.9}$$

$$\frac{\partial \theta_f}{\partial t^*} + \frac{\partial \theta_f}{\partial z^*} = \frac{1}{\tau_r}(\theta_s - \theta_f) \tag{2.10}$$

Where,

$$\tau_r = \frac{u}{H}\frac{\rho_f C_f \varepsilon \pi R^2}{h S_s} \tag{2.11}$$

$$S_s = \frac{f_s \pi R^2 (1-\varepsilon)}{r} \tag{2.12}$$

$r \equiv$ equivalent radius of a rock

$f_s \equiv$ surface shape factor [2-3]

$$h = 0.191 \frac{\dot{m} C_f}{\varepsilon \pi R^2} Re^{-0.278} Pr^{-\frac{2}{3}} \tag{2.13}$$

$$Re = \frac{4 G r_{char}}{\mu_f} \tag{2.14}$$

$$G = \frac{\dot{m}}{\varepsilon \pi R^2} \tag{2.15}$$

$$r_{char} = \frac{\varepsilon d_r}{4(1-\varepsilon)} \tag{2.16}$$

$r_{char} \equiv$ characteristic radius by Nellis and Klein (hydraulic radius)

$d_r \equiv$ nominal diameter of a rock

3.2.2 *Filler material energy balance equation*

In this case, we also substitute the dimensionless variables given in 2.6, 2.7, 2.8 and 2.9 to the energy balanced equation:

$$hS_s(T_s - T_f)dz = -\rho_s C_s(1-\varepsilon)\pi R^2 dz \frac{\partial T_s}{\partial t} \quad (2.17)$$

$$\frac{\partial \theta_s}{\partial t^*} = -\frac{H_{CR}}{\tau_r}(\theta_s - \theta_f) \quad (2.18)$$

Where,

$$H_{CR} = \frac{\rho_f C_f \varepsilon}{\rho_s C_s (1-\varepsilon)} \quad (2.19)$$

3.2.3 *Results of the model for different case studies*

3.2.3.1 Analytical Results: The first simulation was done in a thermocline tank with a chosen geometry, and chosen properties of the filler and heat transfer materials. In the following table 5, one can see the values for each parameter. It is important to remember that the advantage of having reduced the governing equations with dimensionless parameters is that the analysis depends only on two parameters (τ_r and H_{CR}).

ε	τ_r	H_{CR}	H	R	t
0.25	0.0152	0.3051	14.6 m	7.3 m	4 h

Fluid (Therminol® VP-1) properties:

T_h=395 °C	T_l=310 °C
ρ_f=753.75 kg/m^3	C_f=2474.5 J/(kg K)
k_f=0.086 W/(m K)	μ_f=1.8 × 10^{-4} Pa s
$\dot{m}$=128.74 kg/s	

Filler material (granite rocks) properties:

ρ_r=2630 kg/m^3	C_r=775 J/(kg K)
k_r=2.8 W/(m K)	d_r=0.04 m
f_s=3.0	

Table 5. Dimensions and parameters of a thermocline tank [5]

The temperature profiles inside the tank during a discharge process are shown in figure 8. For a discharge process, the bottom of the tank is located in z* = 0 while the hot fluid leaves the tank from the top at z* = 1.

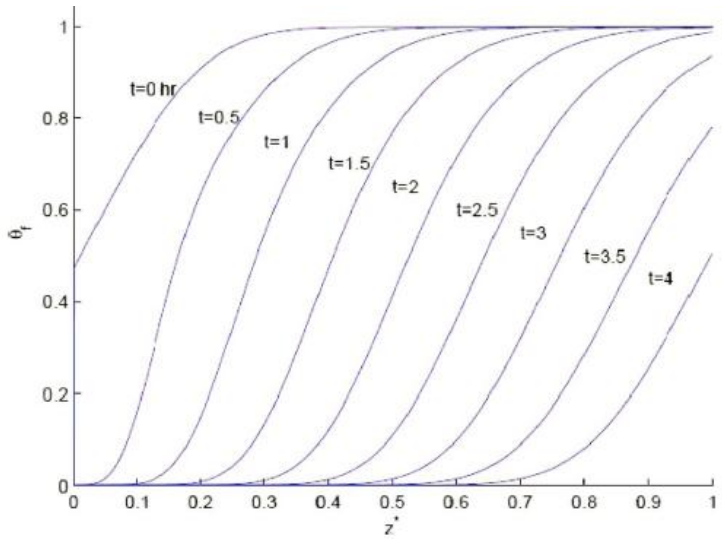

Fig. 8. Dimensionless HTF temperature distribution every 0.5 hours during a discharge process. [5]

The dimensionless temperature distributions presented in figure 8 are the results after 5 cycles of charging and discharging. It was noted that the solution is independent of the initial condition when many cycles take place.

The temperature distribution after 4 hours of discharging or charging is shown in the next figures 9 and 10. It is important to observe that the temperature distribution of the HTF and the filler material are practically the same at the end of the process.

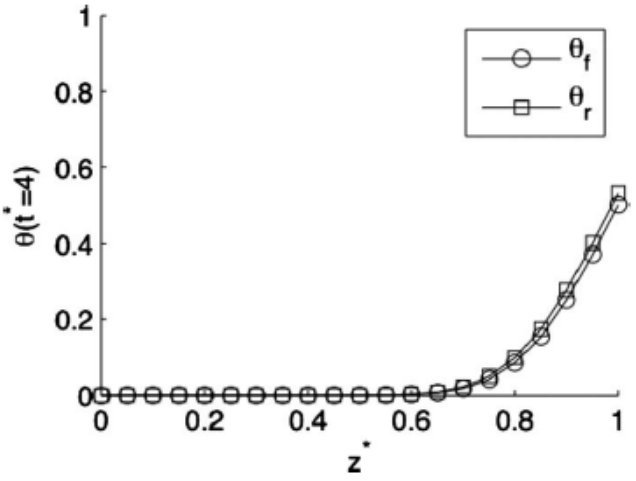

Fig. 9. Dimensionless temperature distribution after 4 hours of discharge. [5]

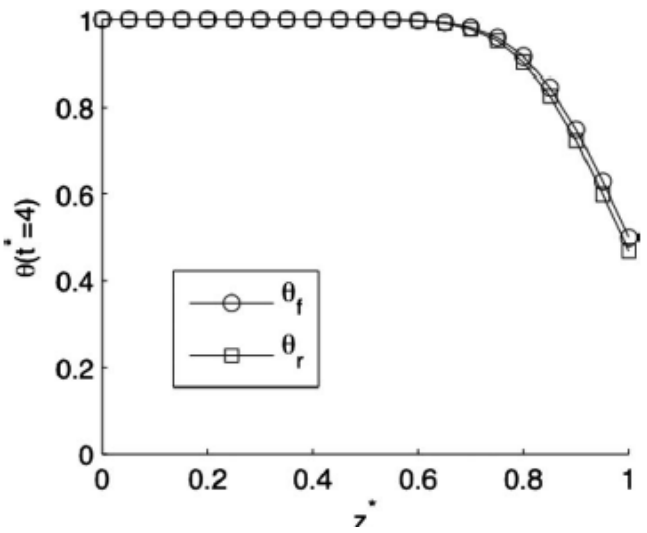

Fig. 10 Dimensionless temperature distribution after 4 hours of charge. [5]

Figure 11 shows the reliability and efficiency of the model depending on the nodes considered. As one can see in the next figure, the dimensionless temperature distribution remains constant for the indicated rank of discretized nodes.

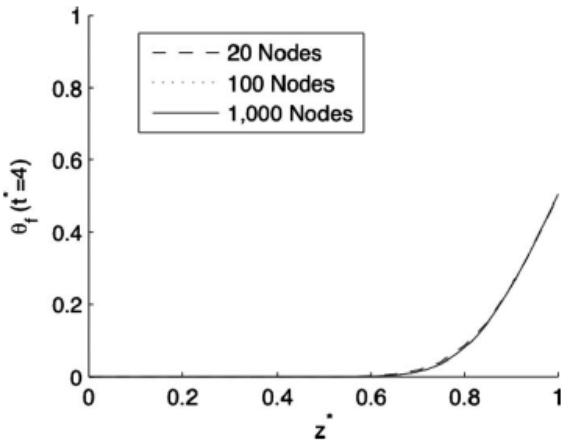

Fig. 11. Dimensionless temperature distribution after 4 hours discharge with different number of nodes. [5]

Finally, it is interesting to know the variation of the HTF temperature at the top of the tank (z* =1) in order to know what is the temperature available in each moment during a discharge or charge process.

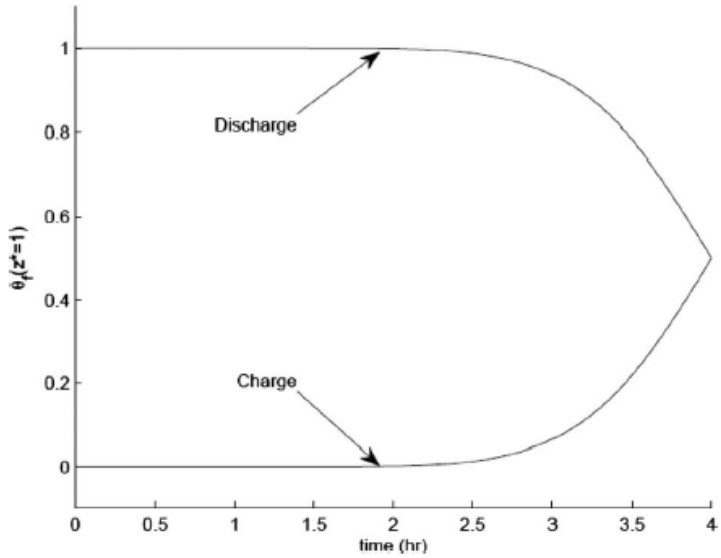

Fig. 12. Dimensionless temperature profile of exit HTF at z*=1 during a discharge and charge process. [5]

3.2.3.2 Experimental Data: The same model was also validated with experimental data in order to improve his reliability. In this case, the storage tank dimensions, and the materials properties were different. The new parameters are listed in Table 6 and the predicted temperatures compared with experimental data are shown in Figure 13.

Fluid (Therminol® VP-1) properties:	
T_h=390°C	T_l=310°C
ρ_f=757.5 kg/m^3	C_f=2464.5 J/(kg K)
k_f=0.0865 W/(m K)	μ_f=1.815×10^{-4} Pa s
$\dot{m}$=25.36 kg/s	
Filler material (granite rock) properties:	
ρ_r=2630 kg/m^3	C_r=775 J/(kg K)
k_r=2.8 W/(m K)	r=0.05 m
ε=0.33	f_s=3.0

Table 6. Dimensions and parameters of a thermocline tank [5]

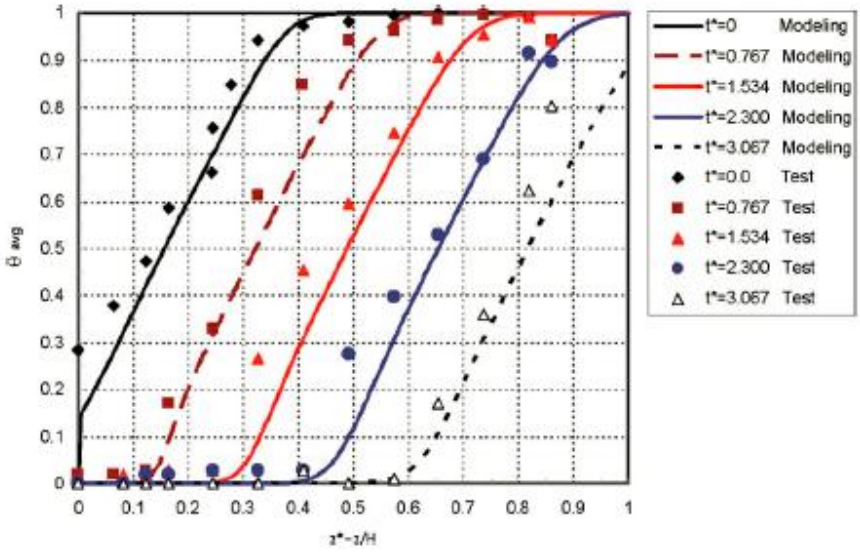

Fig. 13. Comparison of temperature distribution results from the model and experimental data [5]

The temperature distribution from the modelling prediction is considered quite consistent. There were some uncertainties on the properties of materials considered, but the agreement between experimental data and modelling results was considered satisfactory. Therefore, the model was firmly validated.

PART 2

1. Introduction to the model

The software used is MatLab and we use the non dimensional analysis detailed in 3.2 (Part 1) to build the model. The model below is based on the same governing dimensionless equations in 3.2 (Part 1). Therefore, we will use the results plotted in the reference paper in order to validate our model with experimental data. Also, we will try to compare other analytical results. Then, when the model will be validated, we will use it to design an alternative heat storage system for the solar plant, AndaSol I. This storage system will consist on a thermocline tank with Molten Salts as HTF and quartzite rocks as filler material. The thermodynamic properties of these materials are obtained from the reference work [1] which is explained in Part 1, section 3.1.

2. Model development

2.1 Numerical solution [2]

We want to solve two equations with two unknowns. The first equation is the dimensionless governing equations for the heat transfer fluid, and the second one defines the energy balance for filler material. A detailed explanation of how we reach both equations is expressed in 3.2.1 and 3.2.2 from Part 1.

HTF (f):

$$\frac{\partial \theta_f}{\partial t^*} + \frac{\partial \theta_f}{\partial z^*} = \frac{1}{\tau_r}(\theta_s - \theta_f) \tag{2.10}$$

Filler material (s):

$$\frac{\partial \theta_s}{\partial t^*} = -\frac{H_{CR}}{\tau_r}(\theta_s - \theta_f) \tag{2.18}$$

The equations are dependent from time (t*) and 1st order space (z*). Therefore, we want to solve them in order to know the temperatures of the HTF and the filler material in each point of the tank during a period of time. For introducing the equations in MatLab, we use a finite-volume method. The transient term is expressed with a first-order implicit method. Firstly, we define the space first derivative:

$$\frac{\partial \theta_f}{\partial z^*} = \frac{\theta_{f,k+1} - \theta_{f,k-1}}{2\Delta z} \tag{3.1}$$

As the simulation is considered one dimensional in the axis direction, the tank is simulated with N nodes placed vertically in the axis of the tank. The position of each node is expressed by *k*.

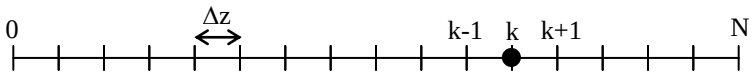

$$\Delta z = \frac{1}{N}$$

$$k \in \{0, N\}$$

Therefore, we define the following matrix for expressing equation 3.1 above and consequently, equation 2.10 changes to equation 3.3.

$$B = \frac{1}{2\cdot\Delta z}^{-1}\begin{bmatrix} 0 & 1 & 0 \\ -1 & \ddots & 1 \\ 0 & -1 & 0 \end{bmatrix} \tag{3.2}$$

$$\frac{\partial\vec{\theta}_f}{\partial t^*} + B\cdot\vec{\theta}_f = \frac{1}{\tau_r}\left(\vec{\theta}_s - \vec{\theta}_f\right) + \frac{1}{2\Delta z}\cdot\begin{bmatrix}\theta_{f,0}\\ 0\\ \vdots\end{bmatrix} \tag{3.3}$$

Moreover, the next step is to define the temporal derivative with finite differential equations. In this case, we used equation 3.4, so that equation 3.3 changes to equation 3.5.

$$\frac{\partial\vec{\theta}_f}{\partial t^*} = \frac{\vec{\theta}_{f,j+1} - \vec{\theta}_{f,j}}{\Delta t} \tag{3.4}$$

$$\frac{\vec{\theta}_{f,j+1} - \vec{\theta}_{f,j}}{\Delta t} + B\cdot\vec{\theta}_{f,j+1} = \frac{1}{\tau_r}\left(\vec{\theta}_{s,j+1} - \vec{\theta}_{f,j+1}\right) + \frac{1}{2\Delta z}\cdot\begin{bmatrix}\theta_{f,0}\\ 0\\ \vdots\end{bmatrix} \tag{3.5}$$

Now, we reordered equation 3.5 putting the terms $\vec{\theta}_{f,t+1}$ in the left side of the equality, and after a few steps, equation 3.8 is obtained from which we know the solution 3.9.

$$\frac{1}{\Delta t}\cdot\vec{\theta}_{f,j+1} + B\cdot\vec{\theta}_{f,j+1} + \frac{1}{\tau_r}\cdot\vec{\theta}_{f,j+1} = \frac{1}{\tau_r}\cdot\vec{\theta}_{s,j+1} + \frac{1}{\Delta t}\cdot\vec{\theta}_{f,j} + \frac{1}{2\Delta z}\cdot\vec{b} \tag{3.6}$$

$$\left(B + \left(\frac{1}{\Delta t} + \frac{1}{\tau_r}\right)\cdot I\right)\cdot\vec{\theta}_{f,j+1} = \frac{1}{\tau_r}\cdot\vec{\theta}_{s,j+1} + \frac{1}{\Delta t}\cdot\vec{\theta}_{f,j} + \frac{1}{2\Delta z}\cdot\vec{b} \tag{3.7}$$

$$A\cdot\vec{\theta}_{f,j+1} = f \tag{3.8}$$

$$\vec{\theta}_{f,j+1} = A^{-1}\cdot f \tag{3.9}$$

Where,

$$\vec{b} = \begin{bmatrix} \theta_{f,0} \\ 0 \\ \vdots \end{bmatrix} \tag{3.10}$$

$$A = \left(B + \left(\frac{1}{\Delta t} + \frac{1}{\tau_r}\right) \cdot I\right) \tag{3.11}$$

$$f = \frac{1}{\tau_r} \cdot \vec{\theta}_{s,j+1} + \frac{1}{\Delta t} \cdot \vec{\theta}_{f,j} + \frac{1}{2\Delta z} \cdot \vec{b} \tag{3.12}$$

A similar, but simpler, procedure is repeated for solving equation 2.18 for the filler material.

$$\frac{\partial \theta_s}{\partial t^*} = \frac{\theta_{s,j+1} - \theta_{s,j}}{\Delta t} \tag{3.13}$$

$$\frac{\theta_{s,j+1} - \theta_{s,j}}{\Delta t} = -\frac{H_{CR}}{\tau_r}(\theta_{s,j+1} - \theta_{f,j+1}) \tag{3.14}$$

$$\left(\frac{1}{\Delta t} + \frac{H_{CR}}{\tau_r}\right) \cdot \theta_{s,j+1} = \frac{1}{\Delta t} \cdot \theta_{s,j} + \frac{H_{CR}}{\tau_r} \cdot \theta_{f,j+1} \tag{3.15}$$

Finally, we should define the initial and boundary conditions for the charging and discharging process. In the charging period, the boundary conditions show that HTF enters from the top of the tank at T_h, while in the discharging period the HTF enters from the bottom of the tank at T_c. Therefore, the initial and boundary conditions for both energy equations are defined respectively as:

- *Discharge process*

$$t = 0, \qquad \vec{\theta}_s = \vec{\theta}_f = f_1(z)$$
$$t > 0, \qquad z^* = 0, \qquad \theta_f = 0$$

- *Charge process*

$$t = 0, \qquad \vec{\theta}_s = \vec{\theta}_f = f_2(z)$$
$$t > 0, \qquad z^* = 1, \qquad \theta_f = 1$$

2.2 Model validation

In this section, the results will be compared with those in section 3.2.3 in order to be firmly consistent on the validity of the model designed.

2.2.1 Contrast with modelling results with experimental data

For this comparison, the model is run with parameters in Table 6 from section 3.2.3, because we have experimental data for this simulation. Figure 14 shows the predicted dimensionless temperature distribution of the HTF obtained with our model every half an hour during 2 hours discharging. One can easily see that the agreement with experimental points is quite satisfactory. Therefore, the model is firmly validated and can be use for new designs and futures studies.

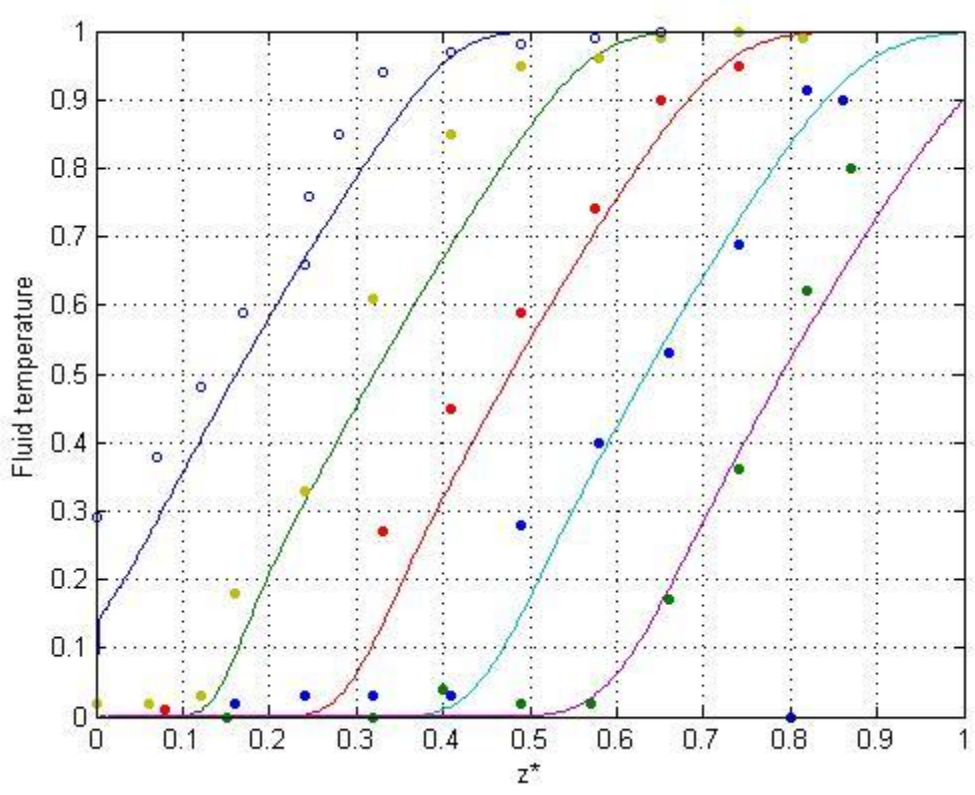

Fig. 14. Comparison of modelling predicted results with experimental data.

Moreover, it is also important to note the agreement with Figure 13, because it characterizes the same simulation.

2.2.2 Contrast with Numerical and Analytical Results

Before using the model for new designs, some other validation studies are needed in order to improve the reliability of the model. In this case, we will repeat the analysis in section 3.2.3.1 and observe both results agree.

Firstly, we simulate the dimensionless fluid temperature in the tank for 5 cycles. Each cycle includes a charge and discharge process which takes 4 hours. Every process is shown in Figure 15 and the dimensionless temperature distribution is plotted every half an hour.

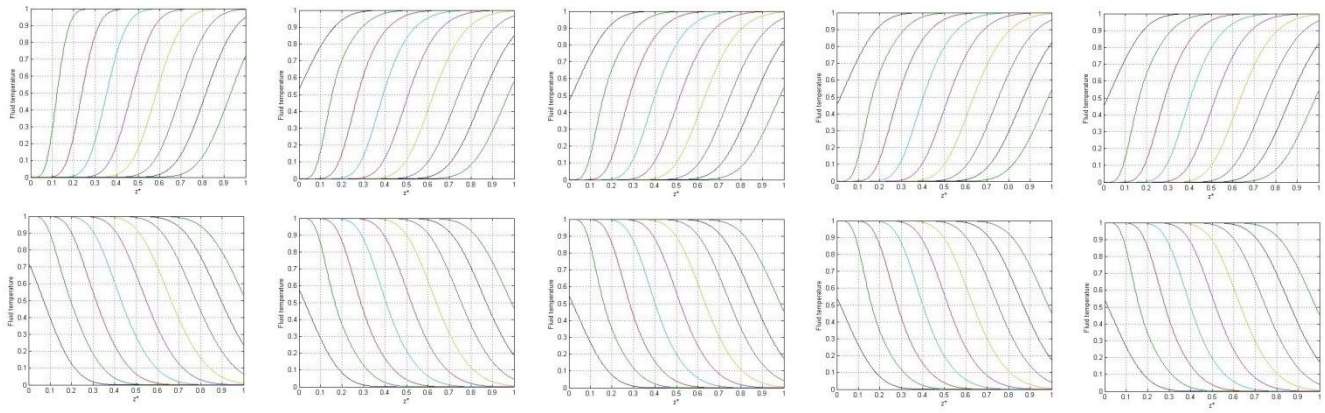

Fig. 15. Dimensionless HTF temperatures distribution every half an hour for discharge and charge processes repeated during 5 cycles.

As one can see in Figure 15, the initial condition does not affect the temperature distribution in the tank. The initial condition of the simulation was an ideal full charged tank, as one can see in the first plot. Nevertheless, the last plots show that after a few cycles, the initial and final temperature distributions remain constant.

Finally, Figure 16 zooms in the common discharge process in order to appreciate the total agreement with Figure 8 in section 3.2.3.1.

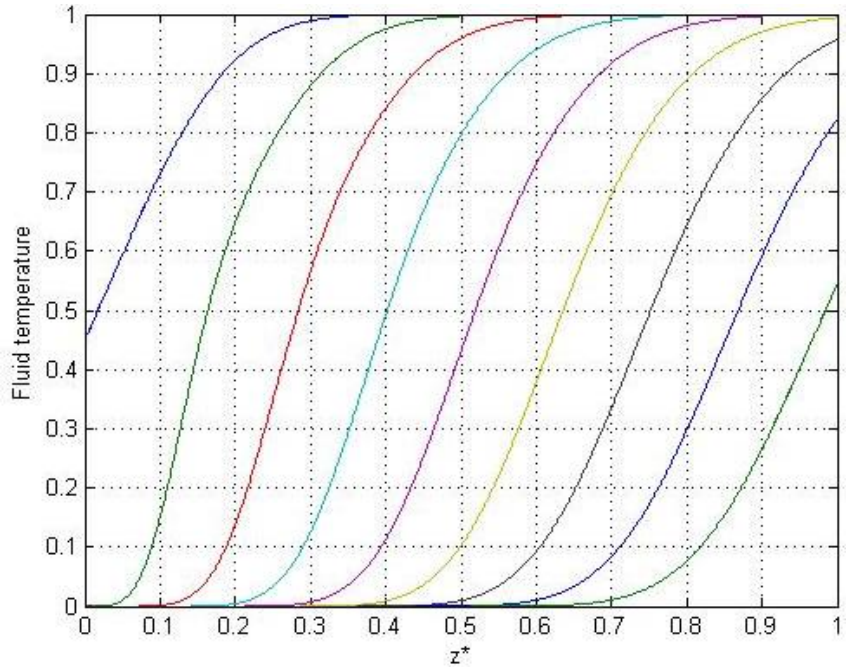

Fig. 16, Dimensionless temperature distribution in the tank every 0.5 hours during a discharge process.

Figure 17 and 18 show the harmony between the HTF and the filler material temperature after discharge and charge process. As it was expected (view Figure 9 and 10), both distributions are practically the same. However, there is a slight temperature difference from z* = 0.7 to z* = 1 caused by the sudden temperature decrease.

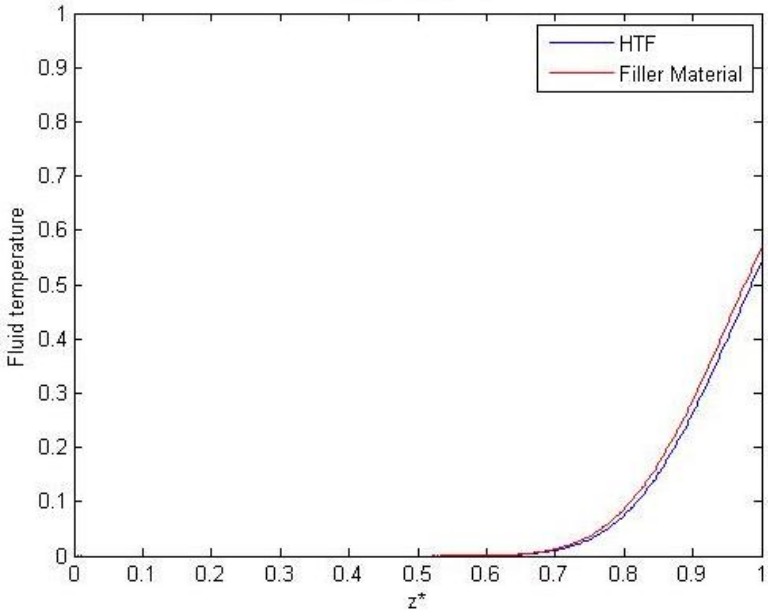

Fig. 17. Dimensionless temperature distribution in the tank after 4 hours of discharge.

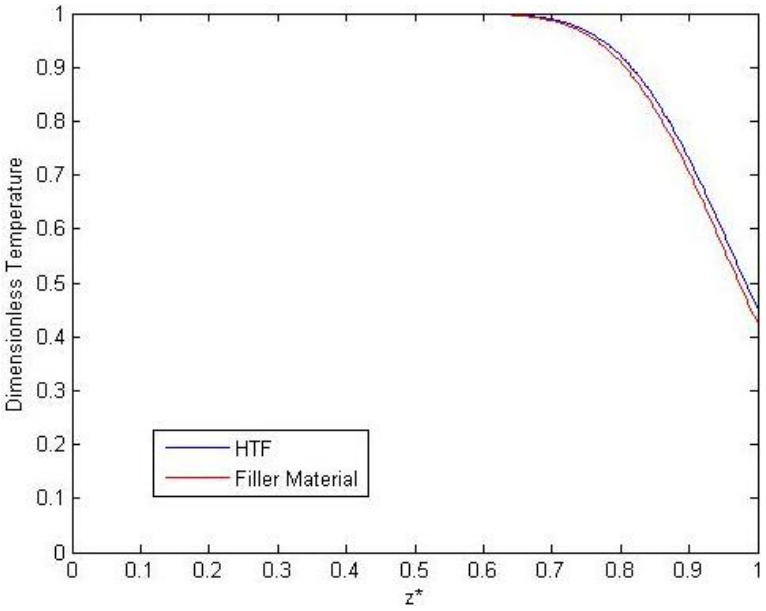

Fig. 18. Dimensionless temperature distribution in the tank after 4 hours of charge.

The next analysis is the influence under different number of discretized nodes in the dimensionless temperature distribution. As one can see in Figure 19, the accuracy of the model is not the same as in the reference work in 3.2.3. That study was accurately from 20 until 1000 nodes, while our model becomes imprecisely when decreasing considerably the number of nodes. However, our model is still accurate between 100 and 1000 nodes.

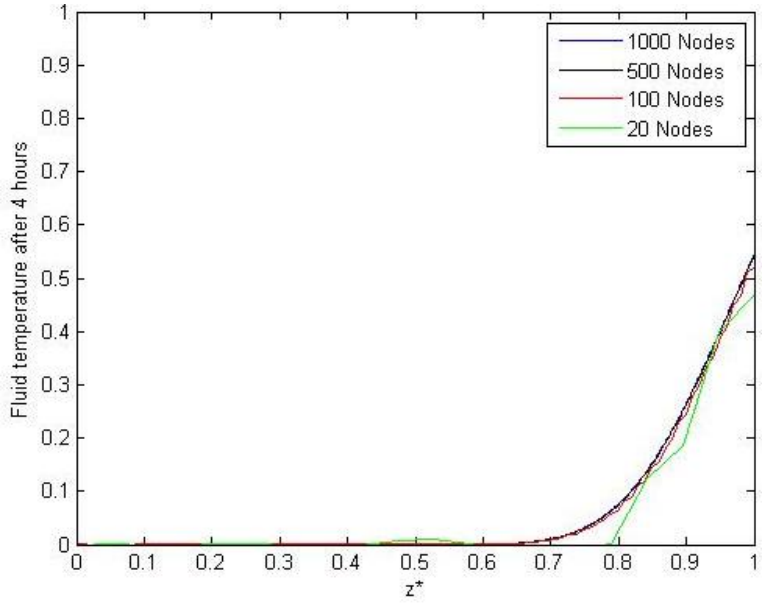

Fig. 19. Comparison of dimensionless temperature distributions after 4 hours discharging under different number of nodes.

PART 3

1. Case study: ANDASOL I [1]

The AndaSol solar power plant is the first solar thermal plant in Europe in which the solar field is based on parabolic solar receivers. It is located in Guadix, a small village in Andalusia (Spain). Moreover, it was built at 1100 m of altitude in a sunny region such that the annual direct insulation is extremely attractive for this type of power plants.

Regarding the storage system, it is used superheated steam as a HTF. The energy of the HTF passes through the storage media with different heat exchangers. In this case, the storage media is molten salts with 40% $NaNO_3$ and 60% KNO_3. Besides this, the storage system consists of two separated tanks: a cold tank at 291 ºC and a hot tank at 384 ºC. Thus, the storage system can be classified as a two tanks indirect system. The storage capacity is about 1010 MWh of heat which allows running the turbine at full-load production of electricity for almost 7,5 hours. However, according to Spanish laws, the solar plant also offers the possibility to use natural gas for producing a 15% of electricity when the storage system is not enough for covering large cloudy periods.

The performance of the plant on a clear summer day is shown in the following Figure 20.

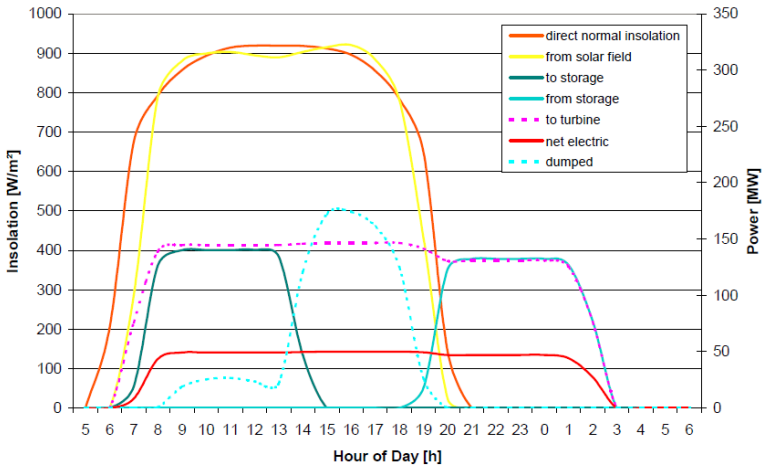

Fig. 20. Insolation and power curves of AndaSol I on a clear summer day [2]

As we can see in the figure above, the storage system allows to produce electricity in a constant way during all the day. Moreover, it is interesting to pay attention on the quantity of energy dumped when the storage systems gets full.

In the next table there is a brief summary about the most important features of the solar plant. These characteristics would be taken into account in the next chapter in the optimization design of an alternative storage system.

ANDASOL I	
Location	37º13'N
Operational hours	3644 h (50 MW_e)
Annual electricity produced	181.831.000 kWh_e
Total efficiency (from solar to electricity)	16 %
Financial investment	260 M €
POWER BLOCK	Rankine cycle
Nominal capacity	50 MW_e
Plant efficiency	37,5 %
Turbine inlet conditions	100 bar and 370 ºC
Turbine inlet conditions (reheat)	16,5 bar and 370 ºC
Nominal steam flow	59 kg/s
Design back pressure	0.08 bar
SOLAR FIELD	Parabolic receivers
Surface	510.120 m^2
Annual direct insolation	2.201 kWh/m^2
T_{in}	292 ºC
T_{out}	392 ºC
Steam production (HTF)	464.703.000 kWh_t
Efficiency from solar radiation to steam production	43 %
STORAGE SYSTEM	Two tanks
HTF	Steam
TES media	Solar Salt (60% $NaNO_3$ 40% KNO_3)
Melting temperature of the molten salts	221 ºC
T_c	291 ºC
T_h	384 ºC
H (each tank)	14 m

D (each tank)	36 m
Storage capacity	1010 MWh_{th}
Storage capacity (hours of full-load production)	7,5 h (at 50MW_e)
Salt mass	28.500 t
Flow rate	948 kg/s

Table 7. Design and working characteristics of AndaSol I [1] [2]

2. Design optimization of an alternative heat storage system

2.1 Procedures of sizing thermal storage tanks [3][4]

The design of a thermocline tank consists on the determination of the size (length and diameter) taking care to satisfy the required energy storage of the solar plant. The size of the storage tank is dictated by the required operational conditions which are:

- Electrical power
- Thermal efficiency
- Operation heat discharge period
- High temperature of the HTF and low temperature of HTF returned
- Properties of HTF
- Properties Filler Material
- Packing porosity

The first step is to consider the tank as an ideal thermocline tank and to calculate the baseline volume for this case. The difference between an ideal thermocline tank and the real one is to consider the presence of a filler material. The presence of a packed bed will explain why the distribution of the temperature is stratified, as it can be seen in Figure 21 below.

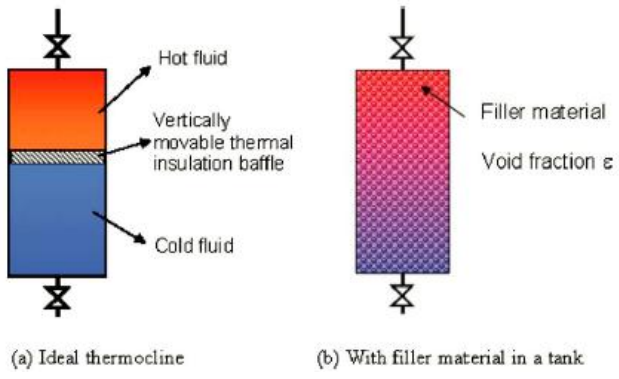

Fig. 21. Illustration of a single tank thermal storage system. [3]

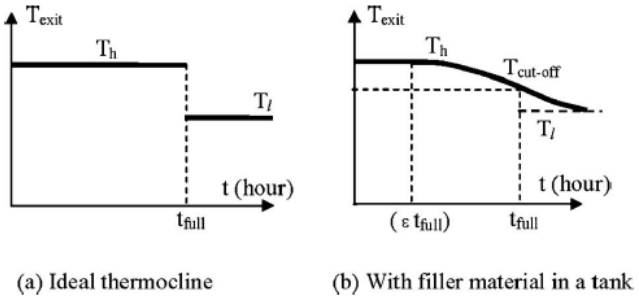

Fig. 22. Distribution temperature during the discharge process when the hot fluid goes out from the top of the tank. [3]

In order to avoid the temperature degradation shown in Figure 22.b, it is necessary to use an ideal thermocline tank or to have a system which stores much more thermal energy than is needed. Thus, during the discharge time period, the temperature degradation would be minimal. However, in a real thermal energy storage system (view Figure 21.b), when the cold fluid is pumped into the bottom of the tank, it extracts heat from the filler material. After some time, the HTF could not heat up because the filler material would become cold as well.

The paragraph above explains why the temperature degradation is inevitable, even if the storage material is fully charged at the beginning. Therefore, in a thermal storage design, the goal is to minimize the temperature degradation, in order that during the required operational period of time ($t_{discharge}$) the temperature of the HTF has minimum degradation from T_h.

The relationship between the volume and the total energy of the tank is expressed on equation 4.1. Moreover, the total energy storage could be estimate with the values of the electric power output, the thermal efficiency of the power plant and operation time period:

$$Q_{total} = V \cdot (\rho C_p)_f \cdot (T_h - T_c) \tag{4.1}$$

$$Q_{total} = \frac{P_e}{\eta_T} \cdot \Delta t \tag{4.2}$$

Moreover, to meet the requirement of minimize the temperature degradation, one needs to store more amount of thermal energy than in an ideal tank. The mathematical expression of this requirement is detailed in equation 4.3.

$$\left[\rho_s C_s (1-\varepsilon) + \rho_f C_f \varepsilon\right] \cdot V_{real} = \left[\left(\rho_f C_f\right) \cdot V_{ideal}\right] \tag{4.3}$$

The second step consists on using a model in order to evaluate the heat transfer and observe the temperature degradation for a full charged tank with packed bed. The model used in this case will be the one designed in Part 2.

The next steps are a trial and error analysis. Therefore, they require an accurate inspection of the results. It is important to observe how change the temperature degradation when the size of the tank is increased, and see if an energy delivery effectiveness of 1 can be achieved. With the results of the analysis, the designer must consider if the temperature degradation is acceptable in relation with the increase of the volume of the tank.

Besides this, the designer can also modify the charge period of time. The discharge period of time cannot be modified because it is considered the required operational time for the plant. If the temperature degradation is not small enough, considering a longer charging time could solve the problem. If not, the size of the tank must be increased again. These last steps can be repeated as long as it is needed in order to come across the optimal values for the volume of the tank and the required increment on the charging time.

Finally, it is important to check if the heat loss from the tank is acceptable with the size of the tank determined before. To compensate the heat loss, the designer could increase the tank size or consider a longer charge time.

2.2 AndaSol I: alternative storage system

2.2.1 First design

First, we determined the minimum required volume for a single storage tank based on ideal thermocline. We use expressions (4.1) and (4.2) in order to know the total heat storage required and the ideal volume.

$$Q_{total} = \frac{50\ MW_e}{0{,}375} \cdot 7{,}5\ h = 1000\ MWh_{th} \tag{4.4}$$

The operation time period is 7.5 hours because it is the same storage capacity of AndaSol plant. Remind that the aim of the project is to optimize the design of the tank maintaining the same required operational conditions. With equation (4.1) we get the ideal volume:

$$V_{ideal} = \frac{Q_{total}}{(\rho C_p)_{fluid} \cdot (T_h - T_c)} \tag{4.5}$$

$$V_{ideal} = \frac{1000\ MWh_{th} \cdot \frac{10^6 W}{1\ MW} \cdot \frac{3600\ s}{1\ h}}{1733 \frac{kg}{m^3} \cdot 1520\ \frac{J}{kg \cdot K} \cdot (384\ ºC - 291\ ºC)} = 14.695\ m^3$$

Moreover, we use equation 4.3 in order to consider a bigger volume which minimizes the temperature degradation.

$$V_{real} = \frac{\rho_f C_f}{\rho_s C_s (1-\varepsilon) + \rho_f C_f \varepsilon} \cdot V_{ideal} \tag{4.6}$$

$$V_{real} = \frac{1733 \frac{kg}{m^3} \cdot 1520\ \frac{J}{kg \cdot K}}{2500 \frac{kg}{m^3} \cdot 830\ \frac{J}{kg \cdot K} \cdot (1 - 0.22) + 1733 \frac{kg}{m^3} \cdot 1520\ \frac{J}{kg \cdot K} \cdot 0{,}22} \cdot 14.695\ m^3$$

$$= 17.611\ m^3$$

The next step is to choose diameter (D) and height (H) that satisfy the minimum volume. With these dimensions, the parameters τ_r and H_{CR} can be evaluated and therefore, the temperature distribution in the tank can be simulated during a discharge process. The dimensions of the tank considered are: H = 15.2 m and D = 39 m.

For choosing these dimensions, we considered the same relation diameter/height than the previous tank which was 36/14 (2.5714).

$$V = \pi \cdot \left(\frac{D}{2}\right)^2 \cdot H = \pi \cdot \left(\frac{D}{2}\right)^2 \cdot \frac{14D}{36} \tag{4.7}$$

$$D = 38.5\,m \rightarrow H = 15.2\,m$$

In the following Table 8, one can see the particular inputs of the model:

H **[m]**	**15.2**
D **[m]**	38.5
ε	0.22
ρ_f **[kg / m^3]**	1733
k_f **[W / (m K)]**	0.57
C_f **[J / (kg K)]**	1520
μ_f **[Pa s]**	0.0021
$\dot{m}$ **[kg / s]**	948
ρ_s **[kg / m^3]**	2500
k_s **[W / (m K)]**	5
C_s **[J / (kg K)]**	830
d_r **[m]**	0.015
T_h **[ºC]**	384
T_c **[ºC]**	291
dT **[h]**	7.5

Table 8. Inputs of the simulation.

The HTF used in AndaSol has the same composition as the fluid used in the case study detailed in 3.1 (Part 1). Therefore, the thermodynamic properties of the HTF and the filler material have been extracted from this literature. Besides this, the flow rate, the hot and cold temperature, and the required time period of energy discharge are operational parameters of the AndaSol plant. Thus, these parameters cannot be modified for the new design.

Surprisingly, the first design has had better results than we expected. In the next Figure 23, one can see the dimensionless temperature degradation of the HTF during different cycles, and each one includes a charge and a discharge process. We observe that 10 cycles are required to stabilize the initial conditions.

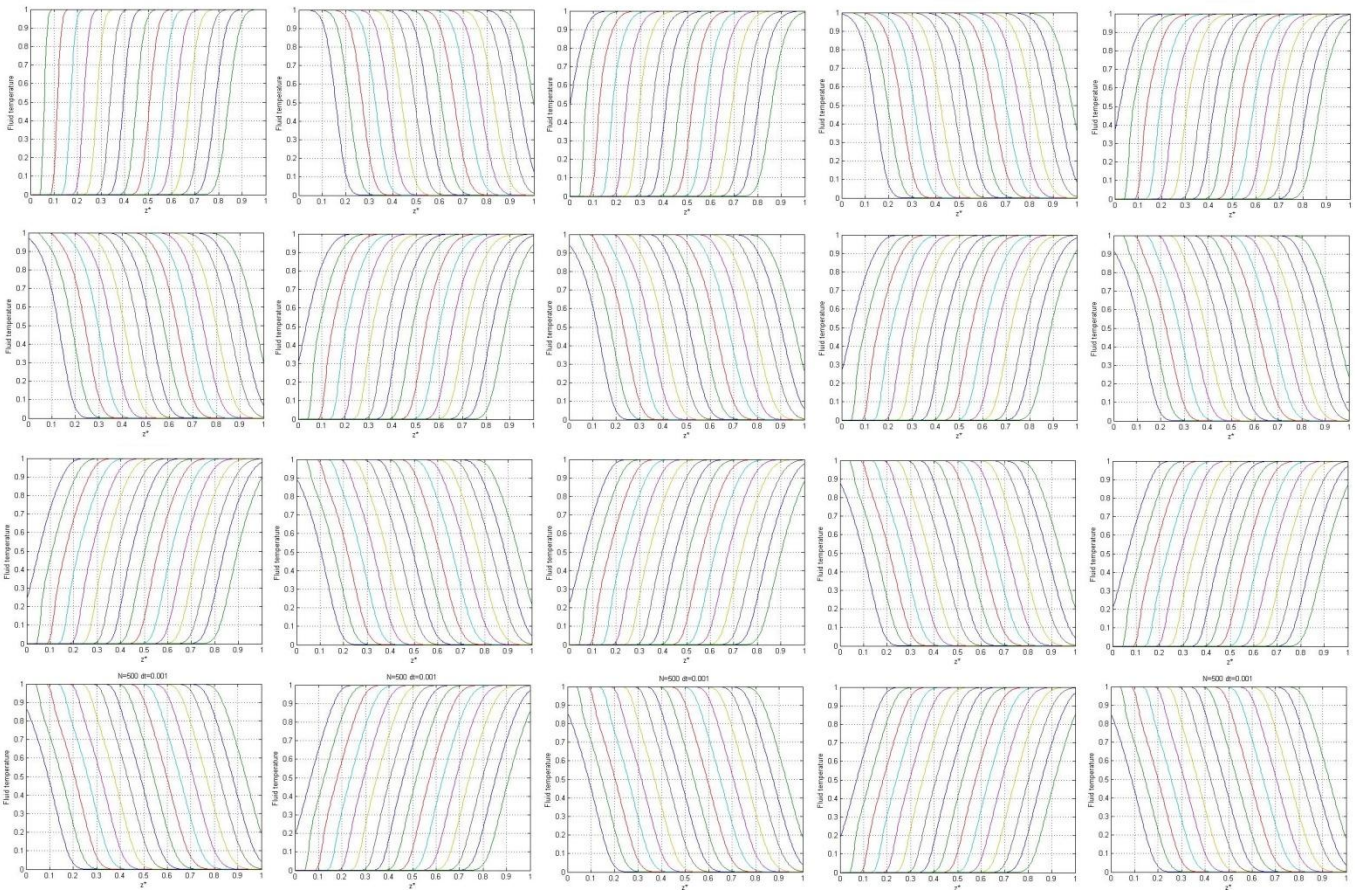

Fig. 23. Dimensionless HTF temperature every half an hour for discharge and charge processes repeated during 10 cycles.

In order to figure out the temperature degradation of HTF during discharge, we plotted the dimensionless temperature histories of exit fluid at z* = 1 during a discharge process. Figure 24 zooms in the dimensionless temperature of HTF during a discharge process while Figure 25 plots the temperature degradation from the same process.

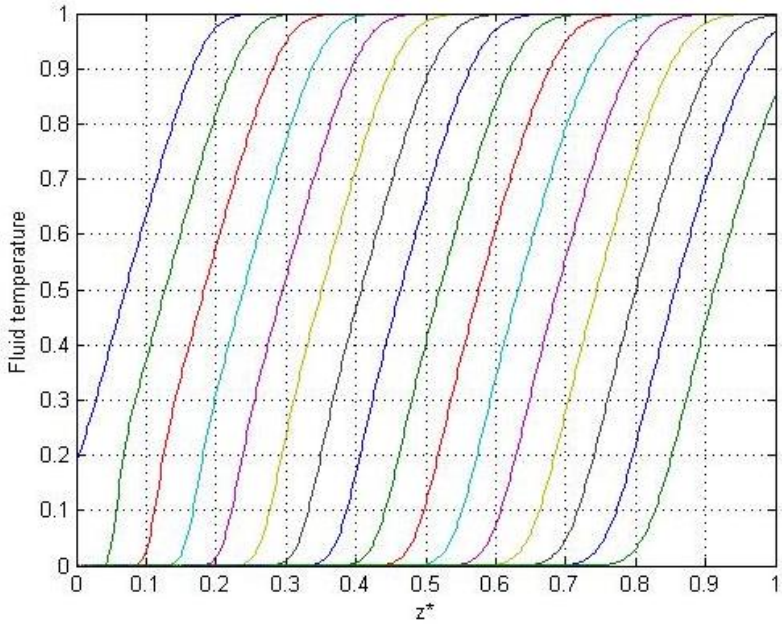

Fig. 24. Dimensionless temperature of HTF every 30 minutes during a discharge process.

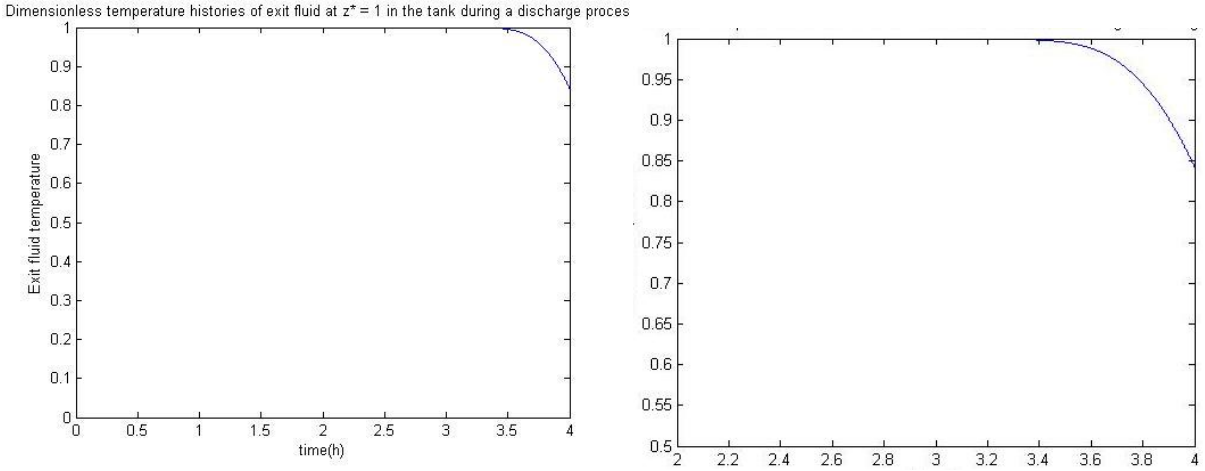

Fig. 25. Dimensionless temperature histories of exit fuid at z* = 1 for a discharge process.

As one can see in the figures above, the temperature degradation is not significant and it seems that this design would work well. However, we will try to improve the design observing the effects produced by the modification of some parameters, always taking into account the thermal energy efficiency which is expressed with the following equation:

$$\eta = \frac{\int_0^{t_{disc\ harge}} \left[T_{f(z=H,t)} - T_L\right] dt}{(T_H - T_L) \cdot t_{disc\ harge}} \qquad (4.8)$$

In the first attempt, the thermal energy efficiency was 0.9928. Therefore, when improving the design, we should pay attention not to deteriorate this parameter.

2.2.2 Optimization of the design: ratio H/D

The first wondering was about the ratio between height and diameter of the tank. We wanted to see if keeping the same storage volume; the geometry could affect the efficiency of the thermal storage. For exploring this question, we simulate again the model above with different ratio values, and we observe the effect on the thermal storage efficiency. Table 9 shows the results for different ratios and Figure 26 plots these conclusions.

H/D	η
0.3948^{*}	0.9928
1.3948	0.9994
2.3948	0.9995
3.3948	0.9995
4.3948	0.9995

Table 9. Thermal storage efficiency under different H/D ratios.

$\left(\frac{15.2}{38.5} = 0.3948^{*}\right)$

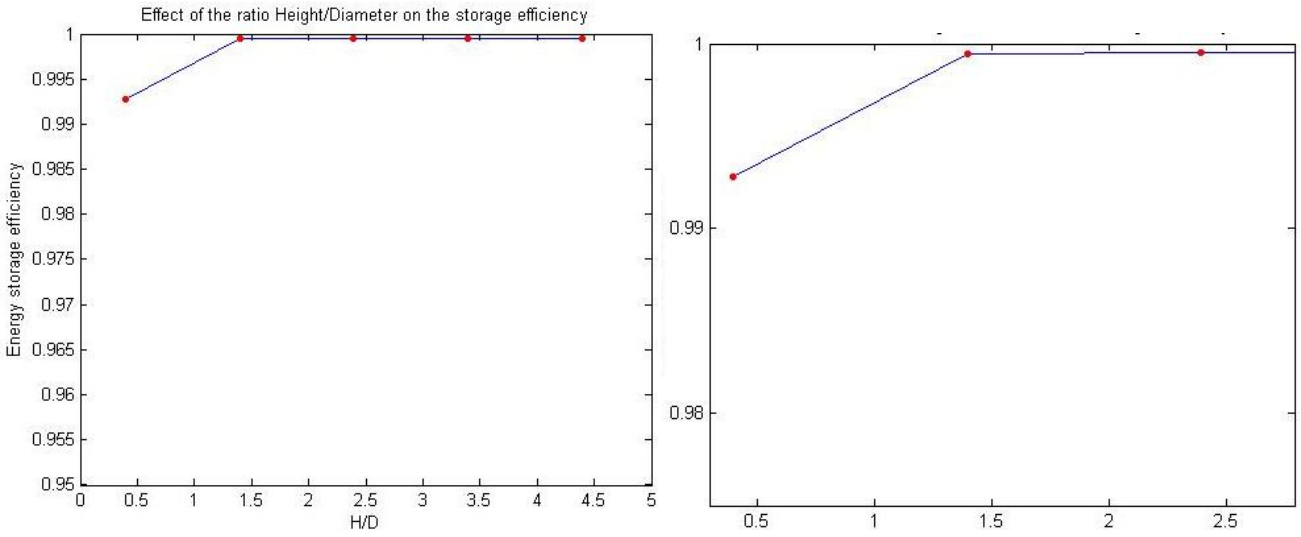

Fig. 26. Effect of the ratio H/D on the thermal storage efficiency.

As one can see, the energy storage efficiency increases with an increase of H/D. In other words, it increases with smaller diameter and bigger height. Moreover, we observe that an efficiency of 1 is reached quickly.

The important conclusion deduced because of this observation is that, if we need to increase the volume of the tank in order to reduce the temperature degradation, it is better to increase it by increasing the height, and consequently, the ratio H/D.

Therefore, the first design in 2.2.1 was modified considering these observations. In order to decrease the HTF temperature degradation, an increase of volume is needed. Thus, we decided to increase the height to 18 m. With this adjustment, the HTF temperature degradation is considerably reduced and the thermal storage efficiency is increased to 0.9992.

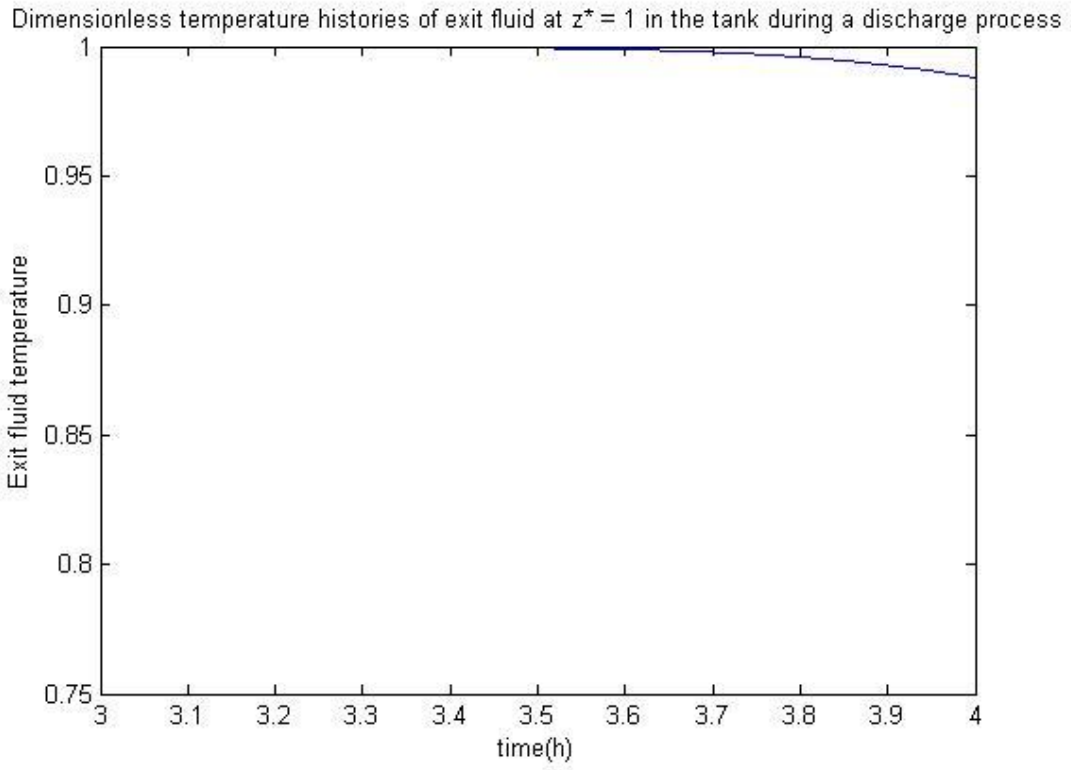

Fig. 27. Dimensionless temperature histories of exit fuid at z* = 1 for a discharge process with the new design.

2.2.3 Optimization of the design: Heat Transfer Fluid [5]

The last investigation is about the HTF. The aim of this last question is to analyze two alternatives to the solar salt as storage fluid. The two fluids selected are called: Hitec XL and Therminol VP-1. The last one is a heat conductive oil already used in the section 3.2.3 (Part 1) from this paper. Besides this, Hitec XL is a molten salt composed with 7% $NaNO_3$, 45% KNO_3 and 48% $Ca(NO_3)_2$. The following Table 10 illustrates the average properties at 300ºC for the thermal energy storage (TES) materials.

TES Materials	**Solar Salt**	**Hitec XL**	**Therminol VP-1**
Density, kg/m^3	1899	1992	815
Heat Capacity, J/kg·K	1460	1800	2300
Thermal conductivity, W/m·K	0.52	0.53	0.21
Viscosity, Pa·s	0.00326	0.00637	0.0002
Melting Point, ºC	220	120	13
Upper Temperature, ºC	600	500	400

Table 10. Properties of two molten salts (Solar Salt and Hitec XL) and one heat conductive oil (Therminol VP-1). [5]

The simulation of the new tank designed previously is repeated for the three storage materials, and the results are shown in the next figures. Each pair of figures is the result of the same simulation, only changing the properties of the HTF. The fluid temperature distribution plotted represents the inside temperature after 20 cycles of charge and discharge process from a fully tank. 20 cycles are required in order to be sure that the initial condition does not affect the temperature distribution.

The melting point and the upper temperature are also indicated in Table 10 because the HTF must work in a temperature range between them in order to stay liquid during the processes required. As T_h is 384 ºC and T_c is 291 ºC, one can see that none of them would have troubles to accomplish this requirement.

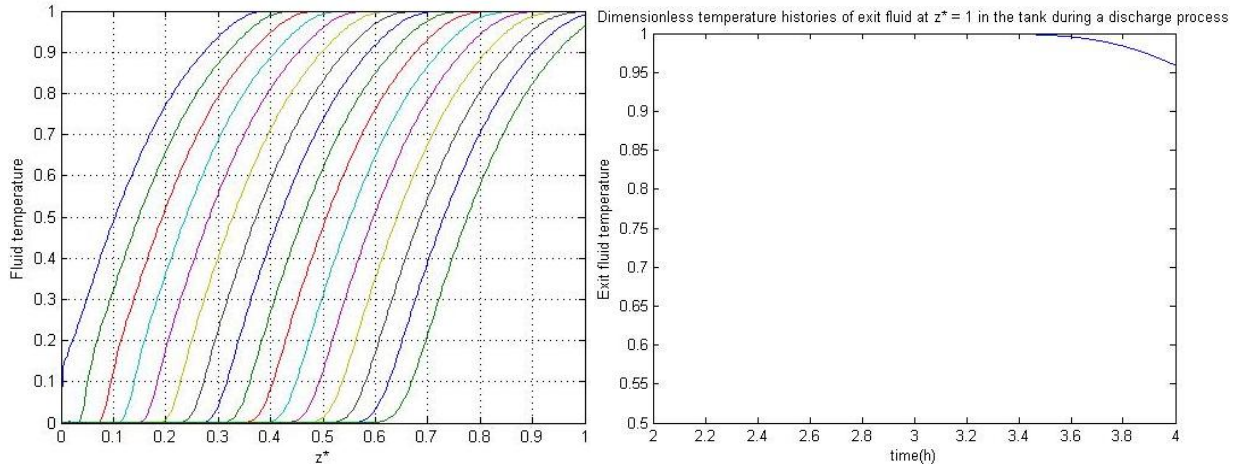

Fig. 28. HTF dimensionless temperature distribution and exit histories at z* = 1 during a discharge process with Solar Salt.

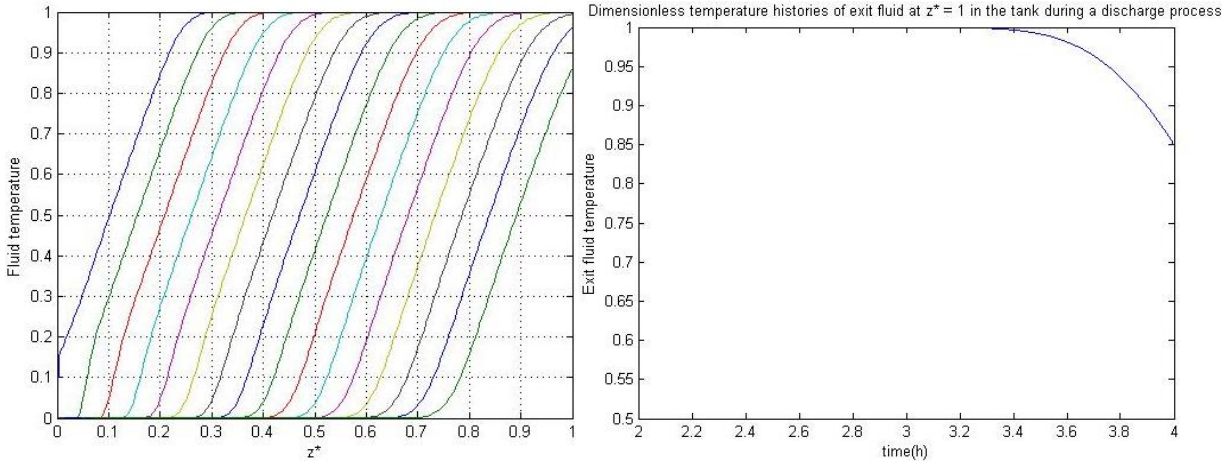

Fig. 29. HTF dimensionless temperature distribution and exit histories at z* = 1 during a discharge process with Hitec XL.

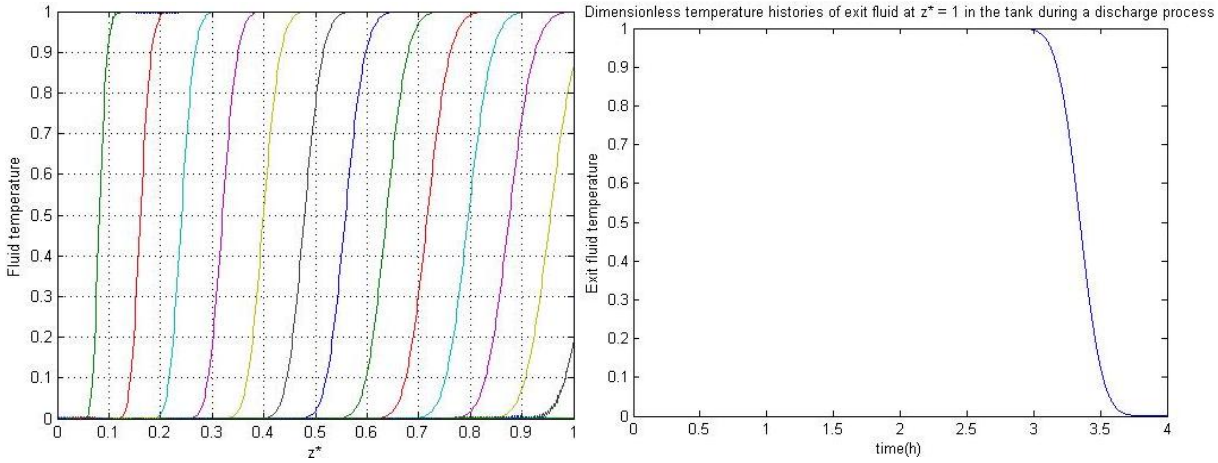

Fig. 30. HTF dimensionless temperature distribution and exit histories at z* = 1 during a discharge process with Therminol VP-1.

As one can see in the figures above, the Solar Salt is the Heat Transfer Fluid which works better for this design because of its lower temperature degradation. Moreover, the temperature degradation of the Hitec XL is not considerable, so that it could be also an effective HTF for this design. Nevertheless, the Therminol VP-1 is totally refused for this tank because the temperature degradation of the HTF is unacceptable for an effective storage tank. The next Table 11 sums up the energy storage efficiency for each example.

HTF	η
Solar Salt	0.9979
Hitec XL	0.9925
Therminol VP-1	0.8369

Table 11. Energy storage efficiency for different Heat Transfer Fluids.

Furthermore, if we consider the cost of each HTF, the Solar Salt becomes also the best thermal energy storage material. As one can see in Table 12, oils use to be much more expensive than molten salts, and consequently, Therminol VP-1 is the most costly. Moreover, between Solar Salt and Hitec XL, the smartest option is the first one.

HTF	Cost of the material ($/kg)	Cost of the heat storage ($/kWh)
Solar Salt	0.49	5.8
Hitec XL	1.19	15.2
Therminol VP-1	2.20	57.5

Table 12. Material and Heat Storage cost for different Heat Transfer Fluids. [5]

CONCLUSIONS

This work introduces different energy storage systems for solar power plants, and presents the modelling of a thermocline storage tank with packed bed. While looking different systems, we understood the advantages of the thermocline tank and his most important parameters.

We obtained and validated a model that can be use for future storage systems designs. Moreover, the model is also useful to investigate the influence of different parameters of the tank. In this paper we studied the influence of the ratio between the height and the diameter of the tank to the thermal storage efficiency. We conclude that an increase in this ratio cause an increase in the thermal storage efficiency. Therefore, this conclusion is useful to take into account when designing thermal storage tanks, because it indicates that it is better to increase the volume by increasing the height than the diameter. The scientific justification is that a smaller diameter corresponds to a higher flow velocity for the Heat Transfer Fluid trough the filler material, and consequently, the heat transfer coefficient would be also higher.

Besides this, the model has been use to propose an alternative storage system for a real solar power plant. AndaSol I has been the solar plant selected because it has a storage system very different from the thermocline storage tank. At the present, it works with two separate tanks which store the hot and cold fluid independently. Thus, a thermocline storage tank would be a low-cost alternative to the currently system, because a single tank requires a lower quantity of materials and space. Finally, a storage system consisting on a thermocline tank with 18 m height and 38.5 m diameter has been obtained as an alternative storage system for AndaSol I. Moreover, this new design offers small fluid temperature degradation. In other words, during all the discharge process, the HTF abandons the tank at T_h.

Furthermore, a comparison between a Solar Salt, Hitec XL and Therminol VP-1 has been completed. This evaluation shows that the best thermal storage material for this design is the Solar Salt. On the one hand, Therminol VP-1 has been refused because of his big temperature degradation and his expensive cost. Moreover, other considerations like environmental concerns or fire hazardous for oils could support the rejection. On the other hand, Hitec XL offers small temperature degradation but still bigger than with Solar Salt. In addition, it is also more expensive. However, if the melting point of the Solar Salt becomes a problem, Hitec XL would be a good alternative because his melting point is lower.

Finally, in order to progress with the optimization of the cost of solar power plants, we would like to propose an innovative idea related with the thermocline storage system. Solar plants work with a common Rankine cycle. For this reason, the plant requires a heat exchanger with a pre-heater, an evaporator and a super-heater. A potential study could be to to assemble the heat exchanger into the thermocline tank in order to reduce the investment cost. The solution could include the tubes of the heat exchanger inside the tank and in conctact with the storage media. Then, the steam would be produced inside of the tubes. However, the governing equation of the model presented in this paper work would be modified in order to consider the heat conduction between the HTF and the tubes.

AKNOWLEDGEMENTS

The author gratefully acknowledges the academic support received from his tutor Mr. Serhat Yesilyurt, and the financial help received from the Erasmus Mundus.

REFERENCE WORKS

Part 1

[1] Gil A, Medrano M, Martorell I, Lázaro A, Dolado P, Zalba B, Cabeza LF. State of the art on high temperature thermal energy storage for power generation. Part 1- Concepts, materials and modellization. Renewable & Sustainable Energy Reviews 2010; pag. 31-55.

[2] Herrmann U, Geyer M, Kearney D. Overview on thermal storage systems. Workshop on Thermal Storage for Trough Power Plants. FLABEG Solar International GmbH; 2006.

[3] Flueckiger SM, Iverson BD, Garimella SV, Pacheco JE. System-level simulation of a solar power tower plant with thermocline thermal energy storage. Applied Energy 2014; pag. 86-96.

[4] Incropera FP, DeWitt DP. Fundamentals of heat and mass transfer. 4th edition. John Wiley & Sons 1996; Chapter 11 Heat Exchangers; pag. 581-619.

[5] Van Lew JT, Li P, Chan CL, Karaki W, Stephens J. Analysis of heat storage and delivery of a thermocline tank having solid filler material. Journal of Solar Energy Engineering; 2011, Vol. 133.

Part 2

[1] Flueckiger SM, Iverson BD, Garimella SV, Pacheco JE. System-level simulation of a solar power tower plant with thermocline thermal energy storage. Applied Energy 2014; pag. 86-96.

[2] Yesilyurt S. Supporting documents for the course “Computational Analysis & Simulation”. Sabancı Üniversitesi.

Part 3

[1] Gil A, Medrano M, Martorell I, Potau X, Cabeza LF. State of the art on high-temperature thermal energy storage for power generation. Part 2- Case studies. Renewable & Sustainable Energy Reviews 2010; pag. 56-72.

[2] Herrmann U, Geyer M, Kistner R. The AndaSol Project. Workshop on Thermal Storage for Trough Power Plants. FLABEG Solar International GmbH; 2002.

[3] Van Lew JT, Li P, Chan CL, Karaki W, Stephens J. Analysis of heat storage and delivery of a thermocline tank having solid filler material. Journal of Solar Energy Engineering; 2011, Vol. 133.

[4] Li P, Van Lew JT, Karaki W, Chan CL, Stephens J, O’Brien James E. Transient Heat Transfer and Energy Transport in Packed Bed Thermal Storage Systems, Developments in Heat Transfer, Dr. Marco Aurelio Dos Santos Bernardes (Ed.), ISBN: 978-953-307-569-3, InTech. 2011.

[5] Energy Storage Technology for Concentrating Solar Power. Center for Clean Energy Technology, Chinese Academy of Sciences. 2011.